LARGE DEFORMATION ANALYSIS OF SHELLS UNDER IMPULSIVE LOADING

A THESIS SUBMITTED TO
THE GRADUATE SCHOOL OF NATURAL AND APPLIED SCIENCES
OF
MIDDLE EAST TECHNICAL UNIVERSITY

BY

MEHMET EVCİM

IN PARTIAL FULFILLMENT OF THE REQUIREMENTS
FOR
THE DEGREE OF MASTER OF SCIENCE
IN
MECHANICAL ENGINEERING

FEBRUARY 2010

Approval of the thesis:

LARGE DEFORMATION ANALYSIS OF SHELLS UNDER IMPULSIVE LOADING

submitted by **MEHMET EVCİM** in partial fulfillment of the requirements for the degree of **Master of Science in Mechanical Engineering Department, Middle East Technical University** by,

Prof. Dr. Canan ÖZGEN _____
Dean, **Graduate School of Natural and Applied Sciences**

Prof.Dr. Süha ORAL _____
Head of Department, **Mechanical Engineering**

Prof. Dr. Haluk DARENDELİLER _____
Supervisor, **Mechanical Engineering Dept**, **METU**

Examining Committee Members

Prof. Dr. Metin AKKÖK _____
Mechanical Engineering Dept., METU

Prof. Dr. Haluk DARENDELİLER _____
Mechanical Engineering Dept., METU

Prof. Dr. Mustafa İlhan GÖKLER _____
Mechanical Engineering Dept., METU

Prof. Dr. Kemal İDER _____
Mechanical Engineering Dept., METU

Prof. Dr. Yavuz YAMAN _____
Aerospace Engineering Dept., METU

Date: 04.02.2010

I hereby declare that all information in this document has been obtained and presented in accordance with academic rules and ethical conduct. I also declare that, as required by these rules and conduct, I have fully cited and referenced all material and results that are not original to this work.

Name, Last Name : Mehmet EVCİM

Signature :

ABSTRACT

LARGE DEFORMATION ANALYSIS OF SHELLS

UNDER IMPULSIVE LOADING

Evcim, Mehmet

M.S., Department of Mechanical Engineering

Supervisor: Prof. Dr. Haluk Darendeliler

February 2010, 101 Pages

In this thesis large deformation behavior of shell structures under high intensity transient loading conditions is investigated by means of finite element method. For this purpose an explicit finite element program is developed with interactive user interface. The developed program deals with geometric and material nonlinearities which stem from large deformation elastic - plastic behavior.

Results of the developed code are compared with the experimental data taken from the literature and simulation results of the commercial finite element

program Ls-Dyna. Moreover, sensitivity study is carried out for mesh size, element type and material model parameters. After the comparison and verification of the obtained results, it is concluded that converged and reasonable results are achieved.

Keywords: Explicit finite element method, nonlinear formulation, impulsive loading, Ls-Dyna Simulation

ÖZ

ANİ YÜKLEME ALTINDA BÜYÜK DEFORMASYONA UĞRAYAN

KABUK YAPILARIN İNCELENMESİ

Evcim, Mehmet

Yüksek Lisans, Makine Mühendisliği Bölümü

Tez Yöneticisi: Prof. Dr. Haluk Darendeliler

Şubat 2010, 101 Sayfa

Bu tez çalışmasında kabuk yapıların yüksek miktarda ve kısa zaman aralığındaki yüklemeler karşısındaki davranışı sonlu elemanlar yöntemiyle incelenmiştir. Bu amaçla, açık zaman entegrasyonu yöntemini kullanan grafik ara yüzüne sahip bir sonlu elemanlar programı geliştirilmiştir. Geliştirilen program, büyük şekil değiştirme ve elastik-plastik malzeme özelliğinden kaynaklanan doğrusal olmayan davranışı hesaba katmaktadır.

Geliştirilen program ile elde edilen sonuçlar literatürde bulunan deney sonuçları ve ticari bir yazılım olan Ls-Dyna programı benzetimleri ile karşılaştırılmıştır. Elde edilen veriler incelendiğinde tutarlı sonuçlara ulaşıldığı değerlendirilmiştir.

Anahtar Kelimeler: Açık zaman entegrasyonlu sonlu elemanlar yöntemi, doğrusal olmayan formülasyon, darbe yüklemesi Ls-Dyna benzetimi

To my Family

TABLE OF CONTENTS

LIST OF FIGURES

FIGURES

LIST OF TABLES

TABLES

NOMENCLATURE

ROMAN LETTERS

B	Strain – Displacement matrix
b	Body Force Vector
C	Constitutive Relation
D	Rate of Deformation, Distance to Charge
DKT	Discrete Kirchhoff Triangle
E	Young`s Modulus, Lagrangian Strain
E_p	Plastic Modulus
F	Deformation Gradient
f_{ext}	External Force
f_{int}	Internal Force
J	Jacobian Matrix
L	Velocity Gradient
L_c	Characteristic Length
N	Shape Function
t	Time
t_a	Time of arrival
w	Displacement in the z Direction, Weight Factor
Z	Scaled Distance
z	Distance from Midsurface

GREEK LETTERS

δ	Kronecker Delta, Deflection
ε	Strain
ε_{eff}	Effective Strain
$\varepsilon_{eff,p}$	Effective Plastic Strain
$\dot{\varepsilon}$	Strain Rate
γ	Gruneisen Coefficient
η	Second Natural Coordinate
σ	Cauchy Stress
σ_J	Jaumann Rate of Cauchy Stress
σ_{yi}	Initial Yield Stress
ω	Rotation of Midsurface
φ	Angle of friction
Ω	Volume
$\dot{\Omega}$	Spin
ξ	First Natural Coordinate
ζ	Area Coordinate

CHAPTER 1

INTRODUCTION

1.1 Impulsive Loading of Structures

Dynamic events are in the area of interest for many disciplines. Although sources of impulsive load may differ, response of the structures to this kind of loading is similar. Behavior of the structure is characterized by the duration of loading (strain rate) and the physical properties of the materials (constitutive relation). Events including crash and impact procedures are characterized by transient response in terms of stress and strain states. The dominant factor is the duration of the impact event. With decreasing duration (increasing strain rate), response of materials diverge from the quasi – static behavior (Figure 1). With increasing the loading speeds inertial forces can`t be neglected. Therefore quasi – static solutions are not applicable for this kind of problems.

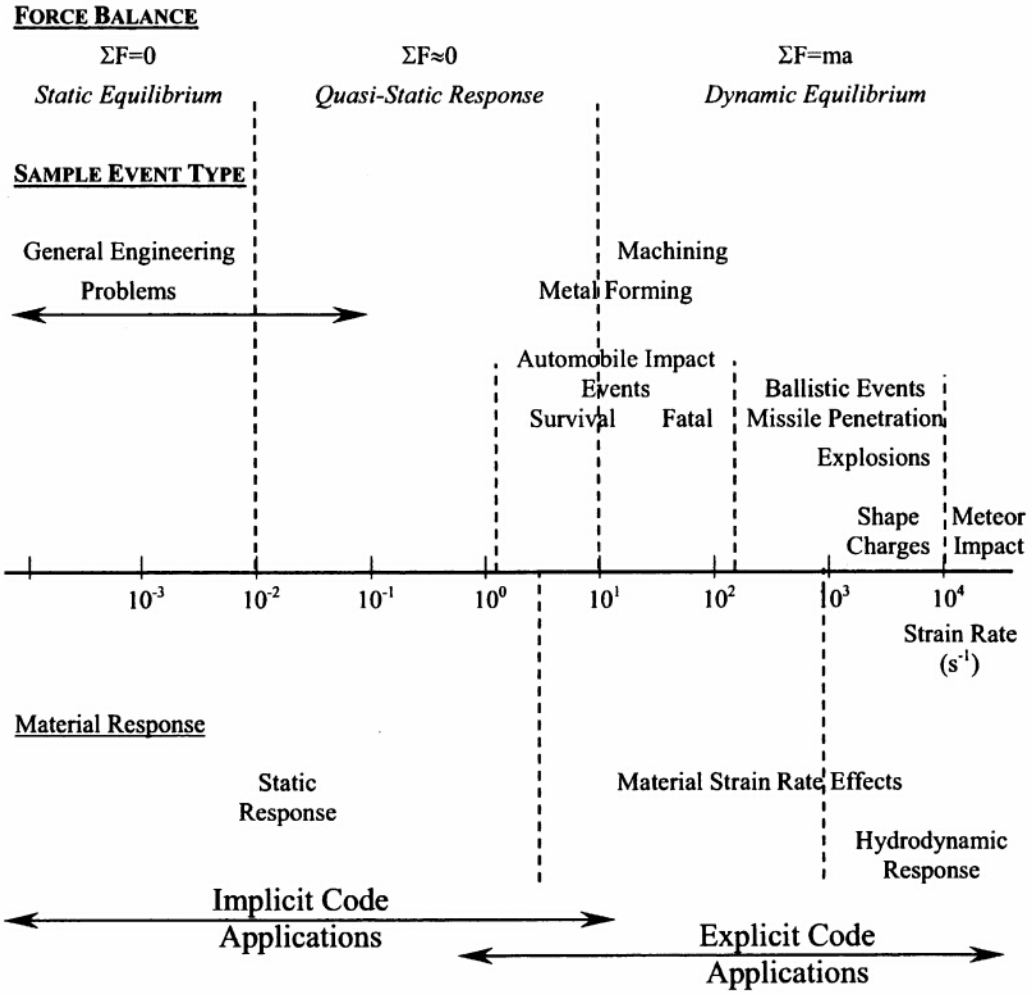

Figure 1: Change of the behavior of materials with increasing strain rate and related simulation method [***1***]

Dynamic behavior of materials is different from that of quasi-static response. When the strain rate increases the material does not have sufficient time to deform. This results in both higher strength (Figure 2) and local deformation (Figure 2).

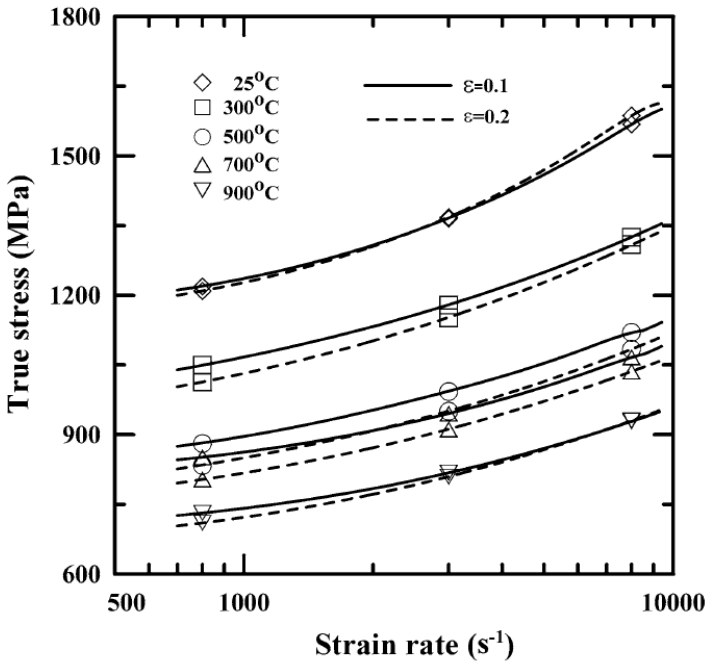

Figure 2: Variation of flow stress with strain rate for a titanium alloy [***2***]

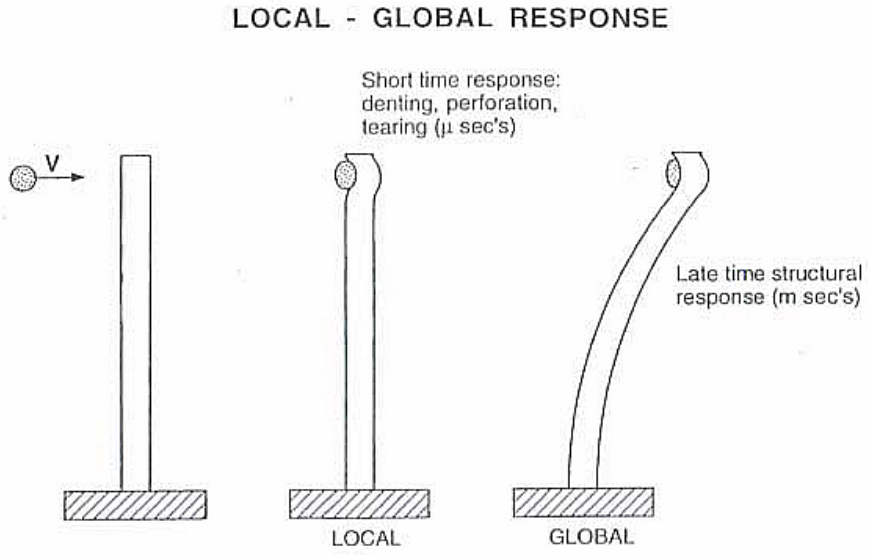

Figure 3: Global to local transition of response of a bar impacted by high speed projectile [***1***]

Typical duration of impact is on the order of seconds for car crash events, several milliseconds for ballistic impacts and microseconds for shaped charge jet impacts. With increasing impact velocities the pressure generated within the structure is increased. As a consequence the response of structures becomes strongly strain rate dependent. When higher strain rates are achieved, the evolution and propagation of shock waves take place. After this point solids behave in a compressible liquid-like (hydrodynamic) manner. Due this phenomenon finite element programs dealing with high speed impact events are called as “hydrocode” [***3***].

In order to solve high speed loading events by means of dynamic deformation and energy dissipation wave propagation phenomenon must be taken into account (Section 3.6.2). Therefore the system equations must be discretised in space and time [***1***].

Duration of a blast load is on the order of milliseconds to microseconds. In addition these loads are ten times or higher than the structural design limits [***4***]. Possible types of impulsive loading are explained in Section 1.1.1.

1.1.1 Sources of Impulsive Loading

Impulsive loading of structures can be caused by many different factors. Most common areas of impulsive loading cases can be listed as follows:

- Automotive
    - Crashworthiness & occupant protection
    - Airbag design
- Defense
    - Ballistic protection and safety of armored vehicles
    - Development of lightweight body armor
    - Weapon development

    - High explosives blast protection
    - Homeland security
- Mining
    - Rock blasting
- Aerospace
    - Bird strike on aircraft structure and engine
    - Engine fan blade out
    - Micro - meteoroid impact on satellite shields
    - Meteoroid impact on planet surface
- Manufacturing
    - Explosive welding
- Metal forming
    - Forging
    - Stamping
- General Consumables
    - Drop test
- FSI applications
    - Atmosphere and water entry vehicles
    - Impact of liquid containers
- Nuclear reactor safety

1.1.2 Blast Loading Phenomenon and Simulation Methodologies

When a high explosive detonates, a pressure front propagates into surrounding atmosphere introducing high levels of pressure waves which are called "*blast waves*". Blast waves are studied in several disciplines including:

- Development of missiles and rockets
- Protection of armored and civilian vehicles from mine and warhead explosions

- Protection of buildings from terrorist attacks

The blast wave is characterized by an instantaneous increase from ambient pressure to peak incident pressure (Figure 4). This strong incident shock wave is characterized by Friedlander equation (for positive phase):

$$P(t) = P_{\max}\left(1-\frac{t-t_a}{t_0}\right)\exp\left(-\beta\frac{t-t_a}{t_0}\right) \qquad (1.1)$$

There are three stages for blast loading of a structure (Figure 4):

- Arrival Duration (t_a): Duration from detonation up to reaching of the blast wave to the structure. Generally for numerical simplicity pressure rise time of the shock wave is assumed to be zero.
- Positive Phase (t_0): Application of the incident high pressure wave on the structure. The damage is mainly caused by the positive pressure load.
- Negative Phase (t_0^-): Contraction of the detonation products and the surrounding air after release of high pressure. Generally this phase does not have any significant effect.

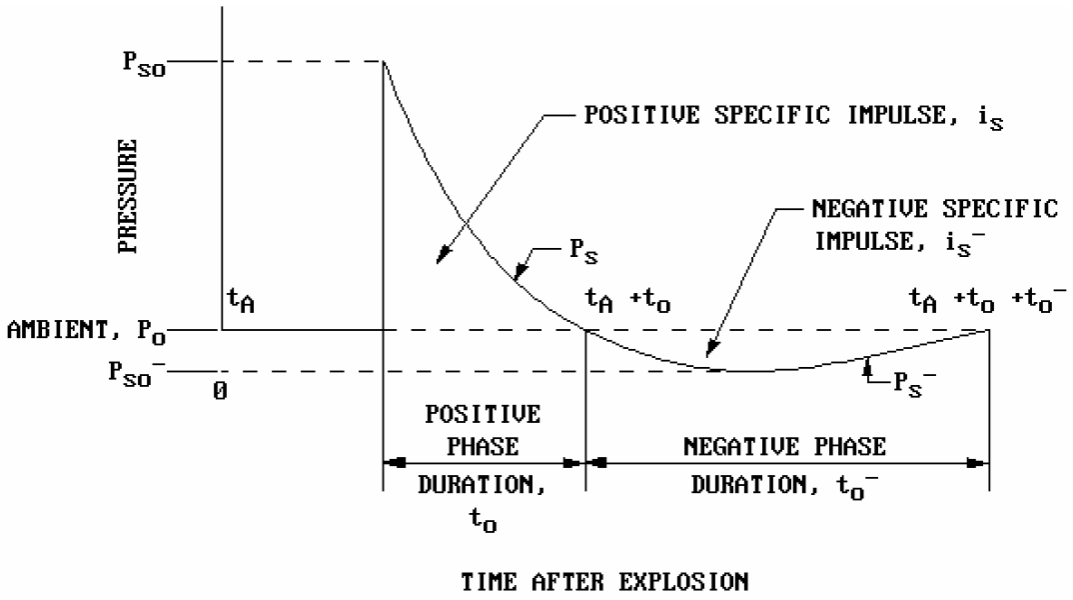

Figure 4: Pressure versus time diagram of a generic blast wave [***5***]

Fist studies on blast loading calculations are based on empirical models due to the complexity of modeling detonation and wave propagation in air. It was observed that the blast load from different amount of explosives at different distances show the same profile. This enables the computation of the structure blast loading are based on previous experiments as functions of the "scaled distance" Z:

$$Z = \frac{D}{\sqrt[3]{W}} \tag{1.2}$$

where D is the distance to the charge and W is the charge's mass. Pressure profile data is generated by using the scaled distance for incident and reflected waves. This methodology concerns only the positive phase of the blast wave [***5***].

However for large deformations which results in failure and fragmentation the above approach is not applicable and a fully coupled simulation is needed. Some techniques to simulate failure of the structure under blast load using coupling are; finite elements, mesh free particles and finite differences. In the case of

coupling both, the fluid dynamical and the structural dynamics regime need to be modeled carefully to cover all relevant effects. In addition, the interaction process may require a specific code module [***3***].

In a case of a uniformly distributed blast load, applied blast pressure is assumed to spread equally over the complete exposed area of the structure. This assumption is used for longer stand-off distances and far-field blasts. For close range detonations, the blast loading is usually considered localized. Thus nonuniform and concentrated pressure distribution must be considered for close range detonations.

Moreover it is difficult to measure the loading and response of the structure as blast load produces high-intensity pressure waves, light flashes and a fireball. As a result of these difficulties, researchers use special instruments for calculating transient displacement or acceleration such as comb-like devices (Figure 19), accelerometers and displacement transducers with high speed data acquisition systems [***4***].

1.2 Scope of the Thesis

The aim of this thesis is to investigate large deformation characteristics of thin structures under impulsive loading situations. A three dimensional nonlinear explicit finite element program is developed for this purpose. The developed program consists of triangular shell elements with five degrees of freedom per node. This element formulation is not implemented to any commercial software yet. Central difference scheme is applied for time integration. Corotational procedure is used with stress rate formulation. A bilinear elastic plastic model is applied to the developed program.

Contents of the thesis study can be summaries as follows:

Chapter 1 explains the aim of the thesis and gives information about dynamic loading and high strain rate behavior of materials. In addition, sources of dynamic loading and characteristics of blast wave are discussed.

In Chapter 2 information is presented about the past studies carried out regarding application of shell elements focusing on the explicit finite element method.

Chapter 3 contains the theoretical information about the finite element method. Firstly types of nonlinearities in finite element method are given. Then large deformation treatment in finite element method is presented focusing on explicit time integration. Brief information about the most commonly used explicit finite element programs is also included.

In Chapter 4 developed code is explained starting from the variational principle. Element formulation, treatment of large deformation and large rotation situation, stress update and plasticity phenomena are explained. Basic functions and the user interface are explained.

In Chapter 5 results of the developed code is compared with the previous experimental data taken from literature and simulation results of Ls-Dyna program. Parametric study is carried out about mesh size, element type, number of through thickness integration point and material model in order observe the dependency of the solution on certain factors.

Chapter 6 concludes the thesis study. Obtained results are discussed and recommendations for further studies are given.

CHAPTER 2

LITERATURE SURVEY

In this chapter previous studies on development of nonlinear finite element methods involving transient dynamic loading are discussed. Attention is focused on triangular shell elements only. To the best knowledge of the author, there is no study available regarding development of 3 dimensional nonlinear explicit finite element program in the national literature.

Mackerle made a bibliographical research on the finite element method applications for static, dynamic, linear and nonlinear analysis including beam, bar, cable, membrane, plate, shell and solid elements. A list of published papers regarding the finite element method for structural analysis can be found in his study [***6***].

Shell elements have been extensively used for thin structures in many engineering problems such as automotive, aerospace, metal forming and high pressure vessels. Their superiority stems from high computational efficiency compared to solid elements.

In the case of hydrocodes, shell elements have larger time step when compared to a solid element of the same thickness. As the through thickness direction is skipped in the calculation, the smallest dimension has no influence on the calculation of the time step. This leads to dramatic time step increases.

Computational efficiency is increased further by reduced integration scheme (which is mostly the case for hydrocodes) using a single Gaussian point [***3***].

Nevertheless shell elements have some disadvantages; they cannot transmit stress waves into the thickness direction. Reduced integration scheme may lead to zero energy modes and deformation patterns which are not associated with strain energy. As a result special numerical treatment (such as hourglass control) is required [***7***].

Two main options of the thin shell theory are implemented in the finite element codes. These are Kirchhoff-Love and Mindlin formulation shells. Kirchhoff-Love shells consider that a normal to midsurface remains straight and normal under deformation of the structure. This assumption does not allow transverse shear formation in the element. On the other hand Mindlin - Reissner shell theory considers normals to the midsurface remain straight but not necessarily normal. In this theory the transverse shear strains are constant throughout the thickness and consequently inconsistent since it is non zero at the free surfaces (bottom and top). This results in overestimation of shear energy. In order to overcome this drawback shear correction factors are used to reduce shear energy [***7***].

In practical applications, generally Kirchhoff – Love elements are more suitable to thin shells whereas Mindlin – Reissner elements are preferred for thick, sandwich or composite plates [***3***].

Batoz developed a triangular plate bending element with only displacement degrees of freedom at the corner nodes using Discrete Kirchhoff Theory (DKT) and a hybrid stress model (HSM) element and a selective reduced integration (SRI) element. He concluded that the most efficient and reliable three node plate bending elements are the DKT and HSM elements [***8***].

Belytschko and Hsiehs developed a finite element for the simulation of transient, large displacement and small strain problems including material nonlinearities. They employed the convected coordinate approach and a direct force calculation for nodes which increased the computational efficiency. They used constant strain triangular and Euler – Bernoulli beam elements. They figured out that the convected coordinate procedure not only simplifies the implementation of complex stress strain laws but also increases the stability and accuracy of the solution [***9***].

Belytschko et al. investigated the performance of various transient finite element methods and developed an efficient computer program for this type of problems. They stated that, when applying explicit time integration scheme to nonlinear problems, computing nodal forces through stiffness matrix does not give efficient computational performance (except for complex elements such as higher order isoparametric type). Direct calculation of nodal forces is made by using derivatives of shape functions. By omitting calculation of a total stiffness matrix they reduced computation and memory costs significantly which allows handling larger finite element models. Also this direct method eliminates the need for a tangential stiffness matrix [***10***].

Stolarski et al. developed a Mindlin plate element using linear fields for rotations and transverse deflections. They separated the displacements into bending and shear modes to achieve better results. This formulation requires single quadrature point for integration which makes it very suitable for the nonlinear explicit finite element method. They reported the accuracy of the element to be similar to the 4 node bilinear Mindlin plate [***11***].

Keulen and Booij developed a curved shell element which has 12 nodal degrees of freedom including corner node displacements and rotations about midsides. They focused on consistent finite rotations with considerable simplifications for

the governing equations which resulted in more efficient implementation of the element. Their formulation is based on the constant strain triangle (CST) and Morley`s element. This element gained significant improvements by additional terms for the membrane deformation. Additional terms can be included by considering elongations of the element sides and change of curvature. They carried out numerical study for sample problems including pulling out of a cylinder and pure bending of a strip [***12***].

Cheung and Zhang developed a nonconforming triangular plate/shell element for geometrically nonlinear analysis. Their formulation has its basis on nonconforming element method for geometric nonlinear analysis. They superimposed Allman's triangular plane element with vertex degrees of freedom and the refined triangular plate-bending element. They reported quite high accuracy for geometric nonlinear analysis of plates and shells [***13***].

Carpenter et al. developed 18 degrees of freedom triangular shell element with improved membrane interpolation. They used DKT bending element to demonstrate the flexural behavior and a plane stress element with a with a new membrane stress formulation to demonstrate the membrane behavior. Membrane stress formulation is established on the basis of a degenerate linear strain triangular. They exploited in plane rotations at each node for this purpose. They concluded that this new element is relatively more efficient and passes plane stress patch test [***14***].

Most of the commercial and academic hydrocodes have the shell element formulation developed by Hughes and Liu. It was the first shell element implemented in Ls-Dyna program. It has objective stress formulation which allows handling large strain problems and was relatively simple and computationally efficient. The element formulation is based on the degenerated brick element which makes it compatible with solid elements [***15***,***16***].

Sabourin and Brunet made an improved formulation of a rotation free triangular shell element for general purpose. The formulation is based on the Morley element which originally expresses the bending behavior with three bending angles only. However they defined the bending angles with rigid body rotations of the element and its neighbors. Membrane effects are approximated by constant strain triangular elements. They carried out several simulations with regular and irregular mesh patterns. They considered large deformations including crash and deep drawing. Deep drawing simulation results indicate that curvatures are captured better as they are imposed by means of translations. Good convergence and accuracy is reported when compared with DKT18 element. The formulated element is implemented in the RADIOSS ® software and suggested for sheet forming simulations [***17***].

Onate et al. extended the rotation free basic shell triangle (BST) to nonlinear analysis of shell structures by explicit finite element method. They used combined finite element and finite volume formulation for the derivation of BST element. An updated Lagrangian scheme and a hypoelastic constitutive law are used for the treatment of nonlinearities. A "control domain" approach is implemented for the formulation of an individual triangle. A constant curvatures field is computed over the triangle in terms of displacements of the six nodes belonging to the four elements patch formed by the central triangle and the three adjacent triangles. They made several benchmarks including large deformation elastoplastic analysis of a spherical dome, cylindrical panel, impact of two cylinders, stretch forming and deep drawing (square box and curved rail). They compared the obtained results with several types of elements such as Stolarski [***11***] and WHAMS-3D explicit finite element code. Good correlation between the results is reported [***18***].

Wu et al. used Discrete Kirchhoff Plate (DKT) element for nonlinear explicit analysis. They made several benchmarks including large twist and crash

simulations. It is stated that DKT element performs well by means of both accuracy and efficiency whereas the 3 node C^0 element is too stiff. Therefore their formulation is used for the formulation of the element stiffness [***19***].

This element is used for the development of the finite element program for the thesis study. Detailed information of this study will be presented in Chapter 4.

CHAPTER 3

FINITE ELEMENT METHOD

3.1 Non-Linear Finite Element Method

There are several types of nonlinearities in structural mechanics such as geometric, material, force and kinematic nonlinearities [***20***,***21***]. Nonlinearities are handled more easily in explicit time integration procedure because of the nature of this method such as:

- A sufficiently small time step is already selected because of the stability condition. Further time step decrease is not needed.
- Inversion of stiffness matrix is not carried out. As a consequence large number of cycles is possible without significant computational cost.

3.1.1 Geometric nonlinearities

Due to large deformation or displacement the strain-displacement equations include higher order terms which produce nonlinear relationships. Strains are not adequately computed using first-order approximations. For strains on the order of 10^{-2}, the error due to small displacement assumption is generally below 1%. But nonlinearity arises for higher displacements [***20***].

3.1.2 Material nonlinearities

The constitutive equation which relates stresses to strains are nonlinear. Inelastic behavior arises from changes in stress-strain relations due to occurrence of plastic yielding. In addition certain materials (especially organic materials such as elastomers) have inherent nonlinear stress response to strain [***20***].

3.1.3 Other Types of Nonlinearity

Other sources of nonlinearities include nonlinear equilibrium effects (i.e. fluid-structure interaction) and contact effects (change in stiffness of the structure) [***21***].

3.2 Large Deformations

For small deformations, the time derivative of the true strain is exactly the rate of deformation. However, in the case of large deformation, the true strain is no longer applicable. The existence of large deformations requires use of objective formulations for deformation terms in order to achieve reference frame independent stresses. Large rotations must be taken into account by rotating the stress tensor [***7***]. When standard time discretization methods are applied to rate constitutive equations in order to achieve objectivity, small time steps are required [***22***].

Objectivity of a finite element formulation is an important issue from the material law point of view. Because the material model must not be dependent on the observer`s position and time. This is the requirement in order to achieve frame indifference to fulfill objectivity [***22***].

Total and updated Lagrangian formulations use different algorithms but the mechanics of the two formulations is same. In addition, total Lagrangian and updated Lagrangian expressions can be converted between each other [***15***].

The basic difference between the two formulations is in the reference point of view. Total Lagrangian formulation defines quantities with respect to the original configuration whereas updated Lagrangian formulation refers to the current configuration (deformed configuration). In addition, stress and deformation measures are treated in different ways. Total Lagrangian formulation adapts a total measure of strain, whereas the updated Lagrangian formulation often uses a rate measure of strain [***7***].

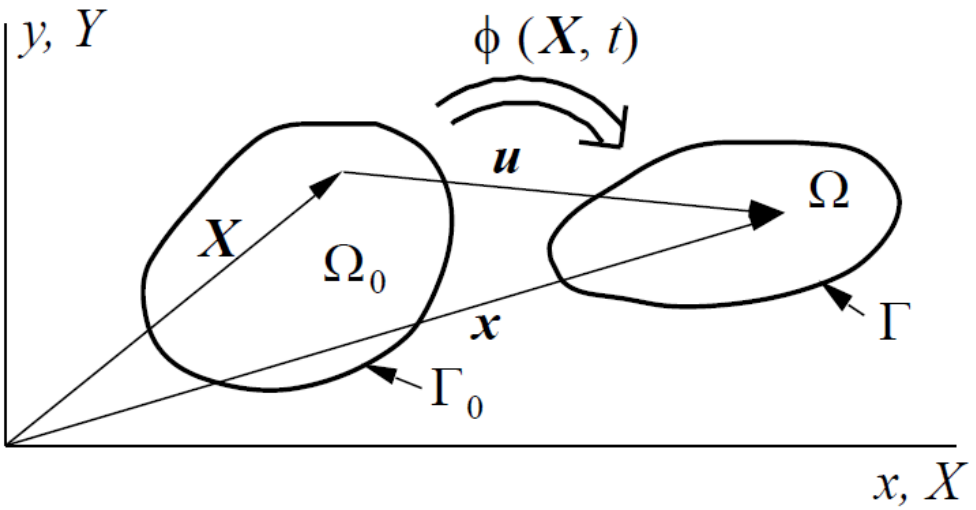

Figure 5: Current and initial configurations of an arbitrary body [***7***].

Since updated Lagrangian approach is more convenient for hydrocodes, attributes of this formulation will be discussed further in below.

3.2.1.1 Updated Lagrangian Formulation

In the updated Lagrangian formulation, the discrete equations are formulated in the current configuration. The stress is measured by the Cauchy (physical) stress. Deformed configuration can be explained by:

$$x = f\left(X, t\right) \tag{3.1}$$

In this method, variables must be expressed in terms of the spatial coordinates x and the material coordinates X in different equations. The dependent variables are chosen to be the stress $\sigma(X,t)$ and the velocity $v(X,t)$. This choice differs from the total Lagrangian formulation, where the displacement $u(X,t)$ is used as the independent variable. This is not a major difference since the displacement and velocities are both computed in a numerical implementation. Equation (3.1) can be inverted to obtain:

$$X = f^{-1}(x,t) \tag{3.2}$$

Any variable can then be expressed in terms of the Eulerian coordinates; for example $\sigma(X,t)$ can be expressed as $\sigma(X(x,t),t)$. While the inverse of a function can easily be written in symbolic form, in practice the construction of an inverse function in closed form is difficult or even impossible. Therefore the standard technique in finite elements is to express variables in terms of element coordinates, which are sometimes called natural coordinates. In Updated Lagrangian formulations, the strain measure is the rate of deformation given by the velocity gradient [***7***].

3.2.1.2 Corotational Formulation

Another approach for overcoming difficulties encountered in large deformation problems is to embed a coordinate system in the element and to rotate with the element. This approach is called Corotational formulation. Embedding a coordinate system at each quadrature point and rotating it with material is valid for large strains and large rotations [***23***]. A key concept in corotational formulation is defining the rotation of the material. Velocity gradient is reported to perform best for explicit finite element method. The consequent formulation accurately represents the behavior of shells and other complex elements [***22***].

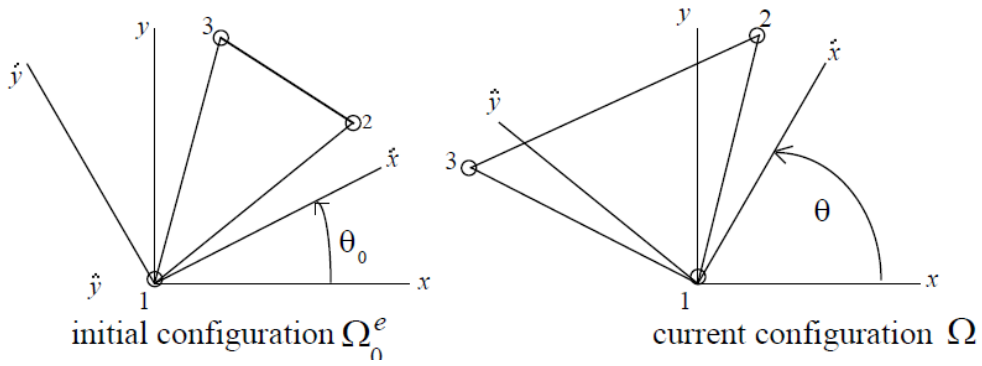

Figure 6: Corotational approach for a triangular element in two dimensions [***7***]

Corotational formulation can be imposed in different ways:

- Polar decomposition
- Rotating the coordinate system referring to a material line in the element (Gives more accurate results than the first approach)
- Rotating the coordinate system referring to a side of the element (Only valid for small strain case) [***7***].

3.2.2 Jaumann Stress Rate

For an explicit scheme the constitutive equations for the strength of the material are expressed as differential equations which must also be integrated in time.

$$\sigma_{n+1} = \sigma_n + \dot{\sigma}_{n+\frac{1}{2}} t_{n+\frac{1}{2}} \tag{3.3}$$

To evaluate the stress rate at $t_{n+1/2}$, the strain rate must be known at that instance. The strain rate is the symmetric part of the velocity gradient $\partial u/\partial x$ (Equation(4.41)). Although the velocity is known at $t_{n+1/2}$, the geometry is known only at t_n and t_{n+1} for the central difference method. A second order approximation to the midpoint geometry is given by the arithmetic average [***24***]:

$$X_{n+1/2} = \frac{1}{2}\left(X_n + X_{n+1}\right) \tag{3.4}$$

3.2.3 Stress Rate in Explicit Time Integration

The procedure used in this section is adapted from [***22***] and [***25***]. The imposed features of the stress update procedure are as follows:

- The formulation is independent of the constitutive model.
- The rate equations are used in an incremental approach (this is also valid for most of the large deformations codes).
- The algorithm is computationally efficient.
- Constitutive models are based on Cauchy stress and defined according to the unrotated reference frame.
- The same methodology can be applied to both three and two dimensions.

The stresses are updated according to the following equations in each time step:

$$\sigma_{t+1} = \sigma_t + \Delta t \dot{\sigma}_J \tag{3.5}$$

$$\sigma_{t+1} = \sigma_t + \Delta t\left(\dot{\Omega}\sigma_t + \sigma_t \dot{\Omega}^T\right) + \Delta t C \dot{\varepsilon} \tag{3.6}$$

$$\dot{\sigma}_J = C_{JC}\dot{\varepsilon} \tag{3.7}$$

Update procedure for displacement, velocity, acceleration, stress and stress rates in time marching scheme of an explicit time integration algorithm is summarized in Figure 7.

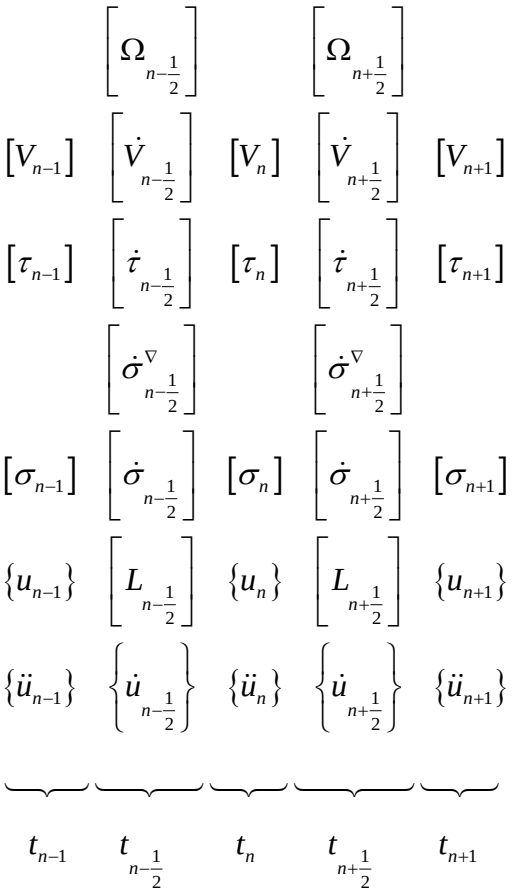

Figure 7: Update procedure by means of time step [***26***]

3.3 Plasticity in the Explicit Finite Element Method

Because of the incremental behavior of the nonlinear explicit finite element method, the solution procedure for plasticity must be in an incremental (rate) form. An incremental elastic - plastic formulation is used to describe the nonlinear material response of metals in most of present finite element codes. The plasticity description for the explicit time integration method is based on the decomposition of the velocity - strain tensor, into elastic and plastic parts [***3***].

The yield function expresses the yield stress in terms of equivalent plastic strain (Equation (3.10)). Equivalent plastic strain is accumulated from the equivalent plastic strain rates as described in the following equations:

$$f_{yield} = \sigma_e\left(I_1, J_2, \theta\right) - \sigma_{yi} \tag{3.8}$$

$$\theta = \frac{1}{3}\sin^{-1}\left(\frac{-3\sqrt{3}J_3}{2J_2^{3/2}}\right) \tag{3.9}$$

where J_2 and J_3 are second and third stress deviator invariants and I_1 is first stress invariant.

Effective plastic strain can be defined in terms of effective plastic strain rate as follows:

$$\varepsilon_{ps} = \sum \delta\dot{\varepsilon}_{ps} = \int \dot{\varepsilon}_{ps} \tag{3.10}$$

where effective strain rate can be calculated by means of strain rate components for two dimensional case as:

$$\dot{\varepsilon} = \frac{2}{\sqrt{3}}\left(\dot{\varepsilon}_{px}^2 + \dot{\varepsilon}_{py}^2 + \dot{\varepsilon}_{px}\dot{\varepsilon}_{py} + \frac{\dot{\tau}_{pxy}^2}{4}\right) \tag{3.11}$$

Hardening for isotropic materials can be introduced by simply changing the fixed yield stress to a variable flow stress [***25***]. Some examples of these functions are summarized in

Table 3.1 and visualized in Figure 8 and Figure 9.

Table 3.1: Various yield criteria [***25***]

Type	**Definition**	
Von Mises	$\sqrt{3J_2}$	(3.12)
Tresca	$2\cos\theta\sqrt{J_2}$	(3.13)
Drucker - Prager	$DI_1+\sqrt{J_2}$	(3.14)
Mohr - coulomb	$\frac{I_1\sin\varphi}{3}+\sqrt{J_2}A(\theta)$	(3.15)

"A" term in Equation (3.15) can be expressed as:

$$A(\theta)=\left(\cos\theta-\frac{\sin\theta\sin\varphi}{\sqrt{3}}\right) \tag{3.16}$$

"D" term in Equation (3.14) is the material constant for Drucker-Prager yield function. φ angle in Equation (3.15) is depicted in Figure 9.

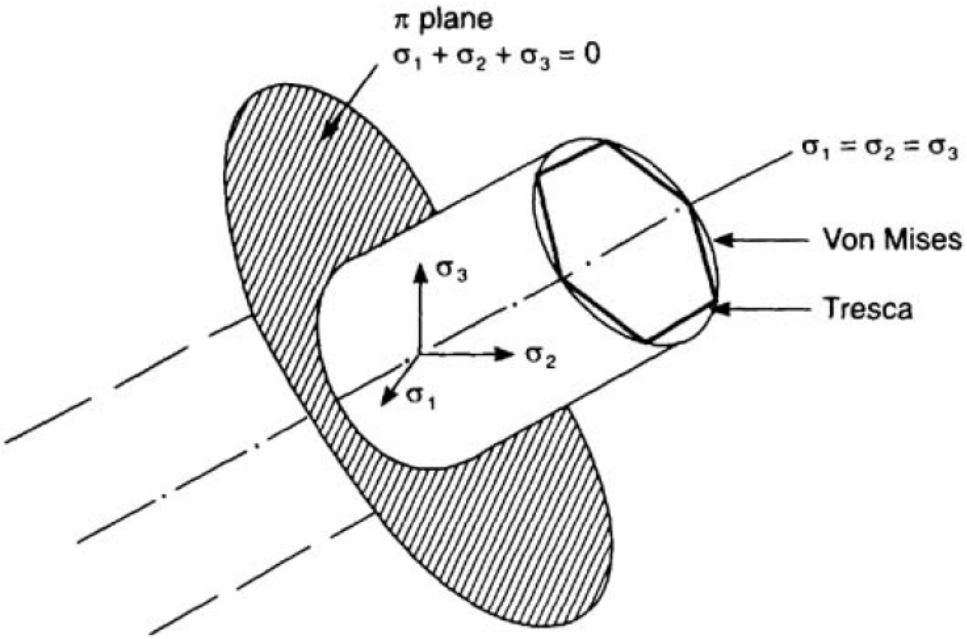

Figure 8: Von Mises and Tresca yield functions [***25***]

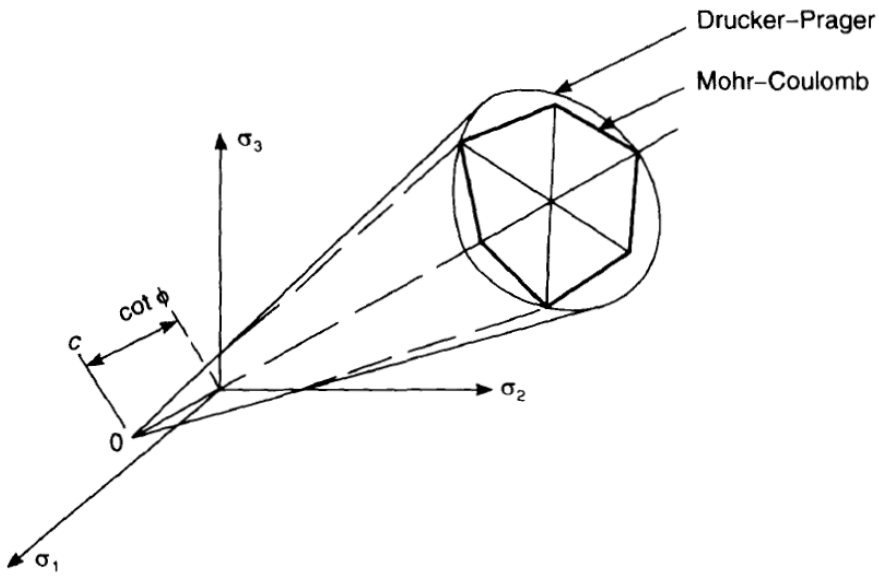

Figure 9: Drucker - Prager and Mohr-Coulomb yield functions [***25***]

3.4 Shear Locking

As a shell element becomes thinner, the shear stiffness term becomes dominant numerically and makes the solution to diverge from the expected thin plate solution. In order to overcome this problem selective reduced integration technique may be used with the standard displacement based elements. The phenomenology behind this method is to under-integrate the shear stiffness terms. For instance in the case of a four noded quad element, the bending stiffness term can be integrated using the 2x2 quadrature whereas the shear stiffness terms can be integrated by a 1x1 quadrature. However when using reduced integration enough integration points must be used in order to maintain additional rigid body modes [***20***].

Another approach to eliminate shear locking is to approximate displacements by higher order polynomials than the rotations. For instance for an eight noded quad element, z displacement can be defined by eight node driven interpolation functions and for rotations Rx and Ry four node driven bilinear interpolation functions [***20***]. This methodology is chosen for the developed finite element code.

3.5 Explicit Finite Element Codes

As discussed in Section 1.1, finite element programs dealing with high speed impact and explosion events are called “hydrocodes” and “wave propagation codes”. The reason stems from the hydrodynamic behavior of materials under intense dynamic loading and formation/propagation of plastic and shock waves in the structure.

First reported hydrocode study was conducted in Los Alamos National Laboratories (LASL) in 1944 for simulating the physical effects of nuclear weapons and it is still kept confidential. Due to very limited computing capacity, early hydrocodes were one dimensional shock tracking codes. Two dimensional codes emerged in the early 1960`s [***27***]. In the meantime Lawrence Livermore National Laboratories (LLNL) developed hydrocodes for investigating high speed contact – impact problems [***28***]. Three dimensional hydrocodes raised a decade later after a significant progress of the computer technology.

In 1980`s hydrocodes become an important tool for crashworthiness and passenger safety simulations in automotive industry. With increasing demand for the computation efficiency, parallelization and domain decomposition procedures were developed and optimized [***29***].

Today`s hydrocodes are capable of handling big finite element meshes (up to several million elements) with efficient domain decomposition algorithms. They can merge different kind of solvers in one problem. Most of the hydrocodes have adaptivity (remeshing) features. Many different material strength and equation of state models are implemented. Moreover some codes allow user defined material models.

Some of the known hydrocodes are Ls-Dyna, Autodyn, MSC. Dytran, Abaqus, Alegra, Pronto, CTH, Epic, Hull, Mesa and Dysmas. A comparison of basic capabilities of the common hydrocodes is summarized in Figure 10.

PRONTO3D	MSC/DYTRAN	MESA	LS-DYNA3D	HULL	EPIC	DYSMAS/ELC	DYNA3D	CTH-EPIC	CTH	AUTODYNE-3D	ALEGRA	ALE3D	Code
●	●		●	●	●	●	●	●		●	●	●	Lagrangian (traditional)
●					●								Smoothed Particle Hydrodynamics (SPH)
													Free-Lagrange Method (FLM)
	●	●		●		●		●	●		●	●	Eulerian
	●			●		●		●					Coupled Eulerian/Lagrangain (CEL)
	●		●							●	●	●	Single-Material Arbitrary Lagrangian/Eulerian (SALE)
	●										●	●	Multi-Material Arbitrary Lagrangian/Eulerian (MMALE)
●	●		●			●	●			●	●	●	Thin-plate Structural Dynamics
●	●	●	●	●	●	●	●	●	●	●	●	●	Small distortion continuum dynamics
●	●	●	●	●	●	●		●	●	●	●	●	Large distortion single-material continuum dynamics
●	●	●		●	●	●		●	●		●	●	Large distortion multi-material continuum dynamics

Figure 10: Main features and application areas of common Hydrocodes [***30***]

3.6 Explicit Time Integration

Detailed information regarding the explicit time integration method will be supplied in Chapter 4.

3.6.1 Solution Procedure

Solution scheme of an explicit time integration method for a hydrocode is as follows:

1- Knowing the stress, pressure, hourglass forces, and shock viscosity at t_n in each zone or element, the forces at the nodes are calculated. The accelerations of the nodes are calculated by dividing the nodal forces by the nodal masses.
2- The acceleration is integrated to give the velocity at $t_{n+1/2}$.
3- The velocity is integrated to give the displacement at t_{n+1}.
4- The constitutive model for the strength of the material is integrated from t_n to t_{n+1} now that the motion of the material is known.
5- The artificial shock viscosity and hourglass viscosity are calculated from $u_{n+1/2}$.
6- The internal energy is updated based on the work done between t_n and t_{n+1}.
7- Based on the density and energy at t_{n+1}, the pressure is calculated from the equation of state.
8- A new time step size is calculated based on the speed of sound through each of the elements and their geometry.
9- Advance the time and return to step 1.

3.6.2 Stability and Critical Time Step

Uncoupling of the equations of motion is the major advantage of explicit integration procedures. No mass or stiffness matrices need be inverted or even assembled, as all the incremental calculations for each degree of freedom can be done independently at the local level. As a consequence nonlinearities are more easily treated in hydrocodes such as material, geometric and contact type. Although number of cycles is very high, computational time per cycle is quite low compared to implicit solution techniques such as Newmark method [***3***].

The time – step is limited by the Courant criterion, i.e. the time it takes the stress waves to travel across one element. This limitation is consistent with the local, uncoupled integration of the equations of motion. If the time-step was larger than the Courant critical value, stress waves would travel across an element within one time - step, affecting the surrounding elements. The incremental behavior of that element would no longer be independent from the rest of the model. The central difference method is considered as the most convenient within the explicit class.

For the explicit time integration, timestep must be sufficiently small in order to achieve numerical stability. Thus explicit time integration is "conditionally stable". However implicit methods are stable even if time step is very large. For a stable time step investigation the system of linear equations of motion can be uncoupled into the modal equations. The detailed derivation can be found in [***31***]. Then the critical time step is calculated as:

$$\Delta t \leq \frac{2}{\omega_{\max}} \tag{3.17}$$

where ω is the natural frequency. It is obvious that the time step is bounded by the largest natural frequency of the structure. However calculating natural

frequency for every single cycle is very costly by means of computational time. As a consequence, using Courant's stability criterion, time step should be determined in a manner such that the information (stress wave) cannot pass over an entire element in one cycle. This critical time step for an element is defined as:

$$\Delta t_c = \frac{L_c}{c} \tag{3.18}$$

where L_c the characteristic length and c is the wave speed in the structure. Characteristic length for plate/shell elements can be determined in two ways [***32***]:

$$L_c = \frac{Area}{Longest\ side\ of\ the\ element} \tag{3.19}$$

$$L_c = \frac{Area}{Longest\ diagonal\ of\ the\ element} \tag{3.20}$$

The sound speed (velocity of the elastic stress wave) in shell elements can be expressed as:

$$c = \sqrt{\frac{E}{\left(1-\nu^2\right)\rho}} \tag{3.21}$$

This value is a function of both the element geometry and speed of sound within the material. For problems involving hypervelocity impact, the impact velocity may exceed the sound speed and smaller time steps must be used. The time step size may also be limited by the contact algorithm, the magnitude of the shock viscosity or an explosive burn [***24***].

3.7 Equation of State Model

In the elastic range, isotropic solids maintain linear pressure - volume change (dilatation) behavior which can be expressed by using bulk modulus as [***33***]:

$$p = -K\Delta V \tag{3.22}$$

However by increasing the intensity of loading and decreasing loading duration the pressure - volume relation becomes nonlinear (Section 3.7.1.1). Formation of high levels of pressures that exceed the material strength generates shock waves in the structure. Shock waves play a dominant role in the deformation behavior. For the reasons mentioned above a decomposition of the volumetric and shear response is needed.

Stress tensor [σ] can be divided into deviatoric [S] and pressure hydrostat [P] terms as follows:

$$\sigma_{ij} = s_{ij} + p\delta_{ij} \tag{3.23}$$

In Eq.(3.23), *p* is defined as:

$$p = \frac{1}{3}\sigma_{ii} \tag{3.24}$$

In matrix form:

$$[s] = \begin{bmatrix} \sigma_{11} - p & \sigma_{12} & \sigma_{13} \\ \sigma_{12} & \sigma_{22} - p & \sigma_{23} \\ \sigma_{13} & \sigma_{32} & \sigma_{33} - p \end{bmatrix} \qquad [P] = \begin{bmatrix} p & 0 & 0 \\ 0 & p & 0 \\ 0 & 0 & p \end{bmatrix} \tag{3.25}$$

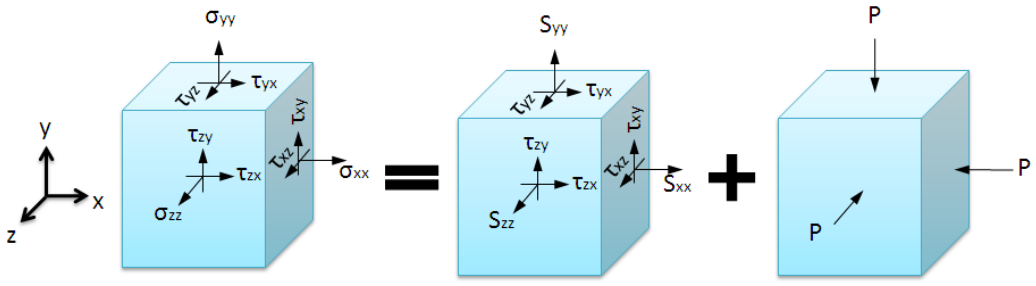

Figure 11: Decomposition of stress tensor into deviatoric and pressure parts

This procedure can also be applied to strain tensor. Deviatoric strain and dilation tensors can be obtained in the same manner, which represent shape change and compression/expansion behavior respectively [***1***].

An equation of state defines the pressure in terms of state variables such as temperature, energy and volume. Shear strength is not considered in an equation of state model. Nonlinear character of response is captured by using equations of state to describe shock waves. In the absence of shock waves, the stress tensor can be described without decomposition [***16***,***3***].

If an equation of state is assigned, material model is used for the deviatoric part and the equation of state is used for the pressure term [***3***]. In this study, equation of state is used for Ls-Dyna simulations with Johnson – Cook material model.

3.7.1.1 Mie – Gruneisen (Shock) Equation of State

This equation of state has its bases on statistical thermodynamics which investigates the material behavior in macroscopic scale as a function of inter - atomic distance. In order to obtain the formulation; a reference state of known pressure, energy and density is used. These values can be obtained by either theoretical approach (i.e. calculation of energy at 0 Kelvin) or experimental data (Shock Hugoniots) [***3***].

Mie-Gruneisen (also known as Shock) equation of state model is suitable for solids under high pressure loads. The pressure load may extend up to 100 kBar. This model describes the pressure in terms of volume and internal energy as:

$$P = \frac{\rho_0 c^2 \mu \left[1 + \left(1 - \frac{\gamma_0}{2}\right)\mu - \frac{a}{2}\mu^2\right]}{\left[1 - (s_1 - 1)\mu - s_2 \frac{\mu^2}{\mu + 1} - s_3 \frac{\mu^3}{(\mu + 1)^2}\right]} + (\gamma_0 + \alpha\mu) E \tag{3.26}$$

where

P : *Pressure*
μ : *Compression*
γ : *Gruneisen Coefficient*
E : *Internal Energy*

The subscript "0" indicates the zero Kelvin status. Detailed information about Mie – Gruneisen EOS can be found in [***3***,***16***].

3.8 Material Models

In this section, concise information regarding the material and equation of state models for Ls-Dyna simulations will be explained. These are Elastic – Plastic Material Model (with and without rate effects option) and Johnson Cook Material Model with Mie Gruneisen Equation of State Model.

3.8.1.1 Elastic – Plastic Material Model

This model is suitable for elastic-plastic material behavior with isotropic and/or kinematic hardening. Due to formulation simplicity it is very effective in terms of computational cost. Furthermore this model requires just a few inputs to characterize elastic-plastic behavior of isotropic materials. Strain rate effects can be considered by using Cowper-Symonds option. As a consequence this model is very popular for elastic-plastic deformation problems.

In the case of isotropic hardening, the center of yield surface is fixed but the radius is a function of the plastic strain. However in kinematic hardening, the radius of yield surface is fixed but the center translates in the direction of plastic strain.

For bilinear case, plastic strain is assumed to change linearly by increasing strain. This phenomenon is implemented by using a constant "plastic modulus" E_p ().

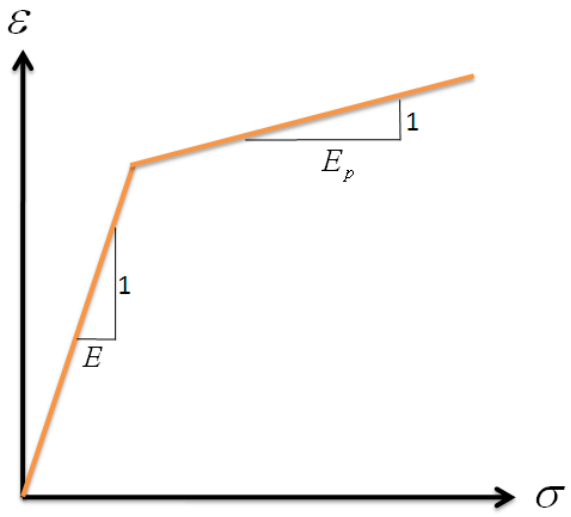

Figure 12: Bilinear elastic plastic material model

3.8.1.2 Johnson-Cook Material Model

The Johnson – Cook model material model is a phenomenological model. It is one of the most used material models for metals. This model is applicable over a wide range of strain rate such as 10^{-3} to$10^{3}\,\mathrm{s}^{-1}$. Recently developed "Modified Johnson Cook Model" can successfully predict material behavior having strain rates up to $10^{5}\,\mathrm{s}^{-1}$. Typical applications include ballistics, high speed impact and explosive loading.

In this model equivalent von Mises flow stress is expressed as a function of strain hardening, strain rate and thermal softening (Eq. (3.27)). These three

affects are assumed to be independent of each other and are combined in a multiplicative manner. This makes Johnson – Cook model relatively easy to develop. By keeping the two parameters constant the other parameter can be determined separately. Johnson Cook model parameters are determined Taylor Impact Test and Split Hopkinson Pressure Bar (SPHB) experiments [***34***].

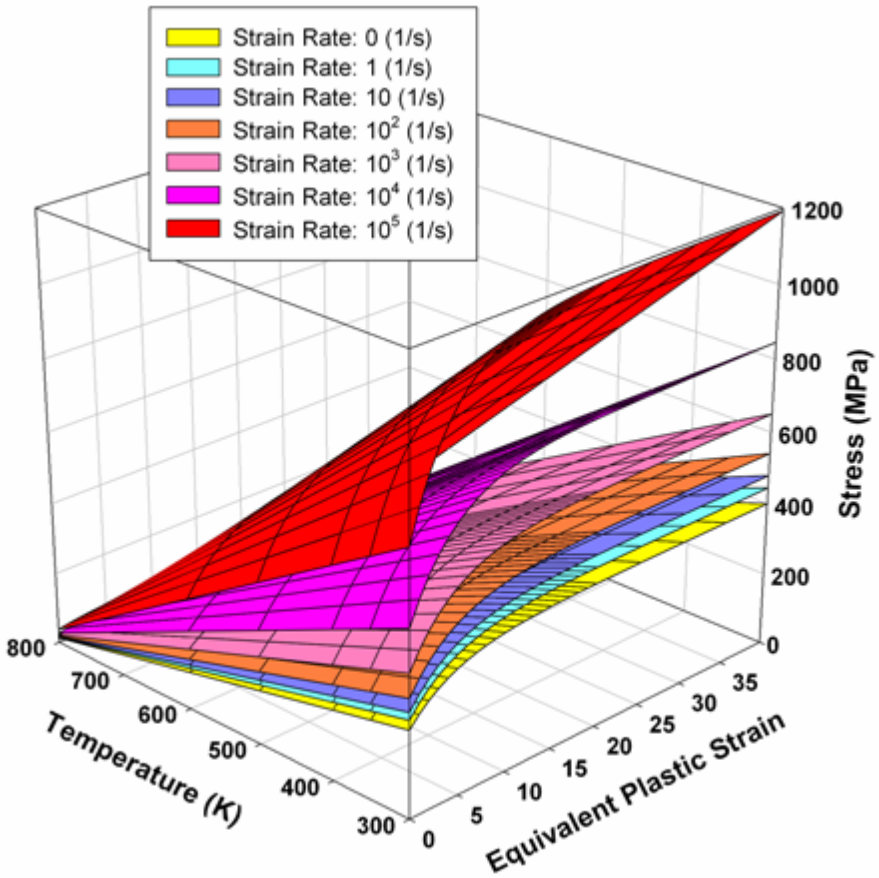

Figure 13: Johnson Cook model parameters plot for Al 356 [***35***]

The flow stress can be expressed as a function of plastic strain, strain rate and temperature as follows:

$$\sigma_{flow} = \underbrace{\left(A + B\varepsilon_{p,eff}{}^{n}\right)}_{\text{Strain Hardening}} \underbrace{\left(1 + C\ln\dot{\varepsilon}\right)}_{\substack{\text{Strain Rate} \\ \text{Effects}}} \underbrace{\left(1 - T_h{}^{m}\right)}_{\text{Thermal Softening}} \tag{3.27}$$

σ_{flow} :Flow stress
A :Initial yield stress
B :Strain hardening constant
$\varepsilon_{p,eff}$:Effective plastic strain
n :Strain hardening exponent
C :Strain rate constant
T_h :Homologous temperature
m : Thermal softening exponent

Homologous temperature is calculated by using Eq. (3.28)

$$T_h = \frac{T_{current} - T_{room}}{T_{melt} - T_{room}} \tag{3.28}$$

Thermal effects are ignored in this study.

3.8.1.3 Cowper - Symonds Model

Cowper and Symonds model is a rate-sensitive elastic–plastic material model which obeys the Von Mises yield criterion. This model scales the yield stress by a strain rate dependent factor as [***16***]:

$$\sigma_{flow} = \left[1 + \left(\frac{\dot{\varepsilon}}{C}\right)^{1/p}\right]\left(\sigma_0 + \beta E_p \varepsilon_{p,eff}\right) \tag{3.29}$$

C and p are user defined constants and $\dot{\varepsilon}$ is defined as:

$$\dot{\varepsilon} = \sqrt{\dot{\varepsilon}_{ij}\dot{\varepsilon}_{ij}} \tag{3.30}$$

Effective plastic strain is calculated by using the following equation [***16***]:

$$\varepsilon = \int_0^t \sqrt{\frac{2}{3}\dot{\varepsilon}_{p,ij}\dot{\varepsilon}_{p,ij}}\,dt \tag{3.31}$$

CHAPTER 4

DEVELOPED EXPLICIT FINITE ELEMENT CODE

In this chapter, developed explicit finite element code will be described in detail. Theoretical detail about the finite element formulation is presented in the previous chapter.

The finite element program is developed by using "Microsoft Visual C# .NET 2008 Express Edition" platform [***36***] and has about 1840 lines of code. For matrix operations including mathematical and file input output processes an open source mathematical library is used [***37***]. Flowchart of the program can be found in APPENDIX B.

The program can handle large elastic – plastic deformations which occur under high intensity transient loading conditions. Several types of conditions can be imposed including time dependent pressure, nodal force, initial velocity and fixed displacements.

4.1 Principle of Virtual Power

Conservation of momentum over a continuum can be expressed as [***7***,***38***]:

$$\sigma_{ij,j} + \rho b_i - \rho \dot{v}_i = 0 \tag{4.1}$$

The weak or variational form for the momentum equation is obtained by multiplying the momentum equation with the virtual velocity δv_i and integrating over the current domain. This gives:

$$\int_{\Omega} \delta v_i \left(\sigma_{ij,j} + \rho b_i - \rho \dot{v}_i \right) d\Omega = 0 \tag{4.2}$$

The first term in Equation (4.2) can be expanded using integration by parts as:

$$\int_{\Omega} \delta v_i \sigma_{ij,j} d\Omega = -\int_{\Omega} \delta v_{i,j} \sigma_{ij} d\Omega + \int_{\Omega} \left(\delta v_i \sigma_{ij} \right)_{,j} d\Omega \tag{4.3}$$

The Gauss divergence theorem can be defined as:

$$\int_{\Omega} A_{ij,j} d\Omega = \int_{\Gamma} A_{ij} n_j d\Gamma \tag{4.4}$$

Then the last term in Equation (4.3) becomes:

$$\int_{\Omega} \left(\delta v_i \sigma_{ij} \right)_{,j} d\Omega = \int_{\Gamma} \delta v_i \sigma_{ij} n_j d\Gamma \tag{4.5}$$

Putting Equation (4.5) in (4.3) gives:

$$\int_{\Omega} \delta v_i \sigma_{ij,j} d\Omega = -\int_{\Omega} \delta v_{i,j} \sigma_{ij} d\Omega + \int_{\Gamma} \delta v_i \sigma_{ij} n_j d\Gamma \tag{4.6}$$

Thus, Equation (4.2) can be expressed as:

$$\int_{\Omega} \delta v_{i,j} \sigma_{ij} d\Omega - \int_{\Omega} \delta v_i \rho b_i d\Omega - \int_{\Gamma} \delta v_i \sigma_{ij} n_j d\Gamma + \int_{\Omega} \delta v_i \rho \dot{v}_i d\Omega = 0 \tag{4.7}$$

This expression is called “principle of virtual power”. It can be summarized as follows:

$$\delta P = \delta P_{internal} - \delta P_{external} + \delta P_{inertial} \tag{4.8}$$

where *P* stands for power.

Finite element interpolation for displacements can be defined as:

$$u_i = N_{ij} u_i^j \tag{4.9}$$

or in terms of velocities:

$$v_i = N_{ij} v_i^j \tag{4.10}$$

where N_{ij} is shape function and the superscript denotes node number.

By dropping the variational degree of freedom v_i and using Equation (4.10), the virtual power expression takes the form:

$$M\dot{v} = f_{external} - f_{internal} \tag{4.11}$$

where

$$f_{external} = \int_{\Omega} \rho b_i d\Omega + \int_{\Gamma} \sigma_{ij} n_j d\Gamma$$

$$f_{internal} = \int_{\Omega} N_{i,j} \sigma_{ij} d\Omega \tag{4.12}$$

$$M = \int_{\Omega} \rho N_i N_j d\Omega$$

After finding accelerations at a specified time "*t*" by solving Equation (4.11), velocity and displacement can be found as follows:

$$v^t = v^{t-1} + \frac{\Delta t^t}{2}\left(\dot{v}^{t-1} + \dot{v}^t\right)$$

$$u^t = u^{t-1} + \Delta t^t v^{t-1} + \frac{\left(\Delta t^t\right)^2}{2}\dot{v}^{t-1} \tag{4.13}$$

where Δt is the time step.

4.2 Mass Matrix of the Triangular Element

Most of the explicit finite element codes use a lumped matrix which results in a diagonal matrix. This matrix is also called as "*lumped mass matrix*".

$$M_{nxn} = \begin{bmatrix} \sum_{i=1}^{n} m_{1i} & & & \\ & \sum_{i=1}^{n} m_{2i} & & \\ & & & \\ & & & \sum_{i=1}^{n} m_{ni} \end{bmatrix} = \begin{bmatrix} m_1 & & & \\ & m_2 & & \\ & & & \\ & & & m_n \end{bmatrix} \tag{4.14}$$

Since the matrix is diagonal its inverse can be calculated by simply taking reciprocals of diagonal elements as:

$$M^{-1} = \begin{bmatrix} 1/m_1 & & & \\ & 1/m_2 & & \\ & & \ddots & \\ & & & 1/m_n \end{bmatrix} \tag{4.15}$$

4.3 Area Coordinates

Area coordinates are widely used when creating shape functions for triangular elements. The use of the area coordinates will directly result in shape functions for triangular elements.

With respect to an arbitrary point P (x,y) in the triangle, area coordinates can be defined as follows:

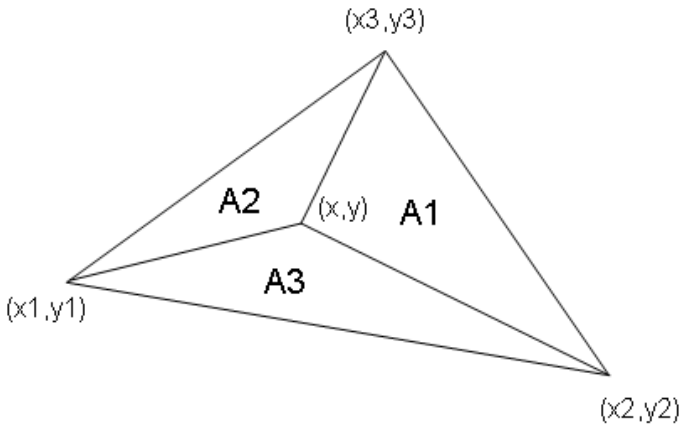

Figure 14: Area partitioning for a triangular element

$$\zeta_i = \frac{A_i}{A} \tag{4.16}$$

$$A_1 = \frac{1}{2}\begin{vmatrix} 1 & x & y \\ 1 & x_2 & y_2 \\ 1 & x_3 & y_3 \end{vmatrix} = \frac{1}{2}\left[\left(x_2 y_3 - x_3 y_2\right) + \left(y_2 - y_3\right)x + \left(x_3 - x_2\right)y\right]$$

$$A_2 = \frac{1}{2}\begin{vmatrix} 1 & x & y \\ 1 & x_3 & y_3 \\ 1 & x_1 & y_1 \end{vmatrix} = \frac{1}{2}\left[\left(x_3 y_1 - x_1 y_3\right) + \left(y_3 - y_1\right)x + \left(x_1 - x_3\right)y\right] \tag{4.17}$$

$$A_3 = \frac{1}{2}\begin{vmatrix} 1 & x & y \\ 1 & x_1 & y_1 \\ 1 & x_2 & y_2 \end{vmatrix} = \frac{1}{2}\left[\left(x_1 y_2 - x_2 y_1\right) + \left(y_1 - y_2\right)x + \left(x_2 - x_1\right)y\right]$$

As a consequence of the above definition, Equation (4.17) is automatically satisfied:

$$\sum_{i=1}^{3} A_i = A \Rightarrow \zeta_1 + \zeta_2 + \zeta_3 = 1 \tag{4.18}$$

Thus area coordinates have the unity property [***39***].

4.4 Natural Coordinates

Natural coordinates are used to locate points within the element by using that element`s geometric properties. These coordinates are used for integration operation over the element area. The dimensionless local coordinates can be expressed as the ratio of the areas:

$$\frac{A_1}{A_{Total}} = \frac{0.5\, s_1\, L_{23}}{0.5\, h_1\, L_{23}} = \frac{s_1}{h_1} \tag{4.19}$$

From Equation (4.19), the value of natural coordinate must be between zero and one. Each point on the triangle can be defined by using natural coordinates.

The x-y coordinates can be expressed in terms of natural coordinates as [***20***]:

$$\begin{aligned} x &= x_{13}\xi + x_{23}\eta + x_3 \\ y &= y_{13}\xi + y_{23}\eta + y_3 \end{aligned} \tag{4.20}$$

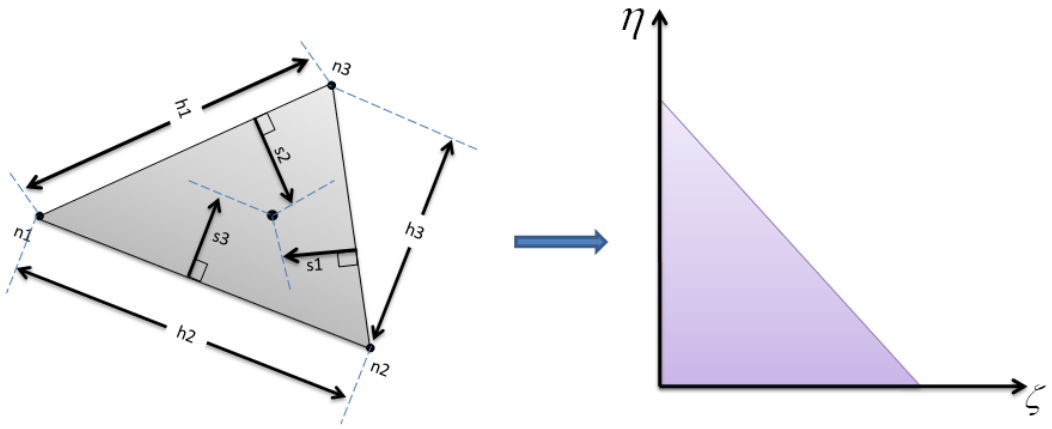

Figure 15: Local triangular coordinates

4.5 Numerical Integration Using Gauss Quadrature

Integrals in finite element formulations are generally complicated and it is not possible to evaluate the integrals in closed form. Thus numerical integration must be used for this purpose. Simple numerical integration rules such as the trapezoidal and Simpson`s rule does not perform well with finite element computation. The “Gauss Quadrature” (also called Gauss-Legendre Quadrature) is more suitable for finite element applications [***20***].

Numerical integration of an area integral over a triangular element can be found using three Gauss quadrature points for integration at the midsides. As the equation for the element shape functions has quadratic terms, a three point Gauss quadrature scheme is sufficient. The points and regarding weight factors for a three point Gauss quadrature are given in Table 4.1.

.

Table 4.1: Gauss quadrature points and regarding weight factors

Integration Point Number	Coordinates	Weight Factor
1	$\left(\frac{1}{2},0\right)$	$\frac{1}{3}$
2	$\left(\frac{1}{2},\frac{1}{2}\right)$	$\frac{1}{3}$
3	$\left(0,\frac{1}{2}\right)$	$\frac{1}{3}$

4.6 Element Formulation

The developed explicit finite element code uses a flat triangular shell element with 15 degrees of freedom. Plate bending (DKT) and membrane element (Constant Strain Triangle) formulations are superimposed. Detailed formulations can be found in the relevant references [***8***,***19***,***14***,***40***].

A corotational approach is implemented with incremental stress rates. At each time step, velocity gradient is calculated. Then the stress increments are calculated from strain increments by the constitutive law.

Displacement of a point in the shell is separated into two components which consist of midsurface part and contribution of rotation, similar to a Mindlin plate as follows:

$$\begin{aligned} U_1 &= u_1 + z\theta_2 \\ U_2 &= u_2 - z\theta_1 \\ U_3 &= u_3 \end{aligned} \tag{4.21}$$

where θ_i is the rotation about the midsurface. Alternatively, Equation (4.21) can be expressed in terms of velocity as follows:

$$
\begin{aligned}
V_1 &= v_1 + zw_2 \\
V_2 &= v_2 - zw_1 \\
V_3 &= v_3
\end{aligned}
\tag{4.22}
$$

where w_i is the angular velocity.

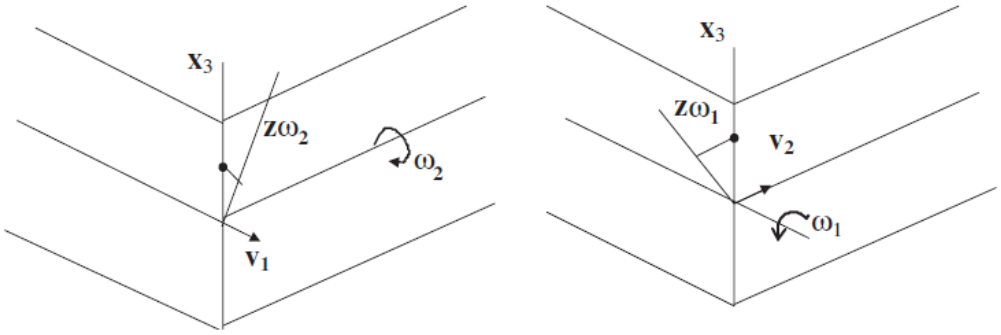

Figure 16: Velocity of a point depending on the distance from midsurface [***19***]

Formulation of the constant strain triangle element is simple and well known. Nodes have only translational degrees of freedom in x and y directions for the in plane contribution. Shape functions to define midplane velocities, v_1 and v_2, are expressed as [***41***]:

$$
\begin{aligned}
\varphi_1 &= 1 - \zeta - \eta \\
\varphi_2 &= \zeta \\
\varphi_3 &= \eta
\end{aligned}
\tag{4.23}
$$

Then

$$
\begin{aligned}
v_1 &= \varphi_1 v_1^1 + \varphi_2 v_2^1 + \varphi_3 v_3^1 \\
v_2 &= \varphi_1 v_1^2 + \varphi_2 v_2^2 + \varphi_3 v_3^2
\end{aligned}
\tag{4.24}
$$

Shape function formulation for the DKT plate bending element is based on the study of Batoz et al [***8***]. Shape functions for angular velocities w_1 and w_2 can be expressed in terms of natural coordinates as follows:

$$
\begin{aligned}
\psi_1 &= 2(1-\zeta-\eta)(1/2-\zeta-\eta) \\
\psi_2 &= \zeta(2\zeta-1) \\
\psi_3 &= \eta(2\eta-1) \\
\psi_4 &= 4\zeta\eta \\
\psi_5 &= 4\eta(1-\zeta-\eta) \\
\psi_6 &= 4\zeta(1-\zeta-\eta)
\end{aligned}
\tag{4.25}
$$

In order to calculate the transversal velocity v_3, the element uses 2-node Hermite cubic interpolation along each side Figure 17.

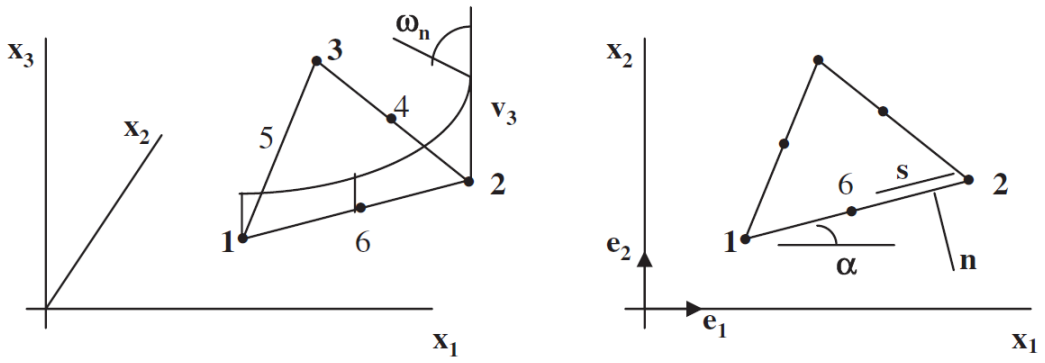

Figure 17: Geometry definition at the side [***19***]

For instance by taking "s" between 0 and 1 through side 1 with nodes 1 and 2, the transversal velocity can be found from the following relations:

$$
\begin{aligned}
v_{3|_{side1}} &= v_3^1\chi_1 + v_3^2\chi_2 + \left(v_{3,s}\right)^1\chi_1^1 + \left(v_{3,s}\right)^2\chi_2^1 \\
\chi_1 &= 1-3s^2+2s^3 \\
\chi_2 &= 3s^2-2s^3
\end{aligned}
\tag{4.26}
$$

$$
\begin{aligned}
\chi_1^1 &= \left(s-2s^2+s^3\right)L \\
\chi_2^1 &= \left(-s^2+s^3\right)L
\end{aligned}
\tag{4.27}
$$

Thus angular velocity can be expressed by taking L as the side length:

$$w_n = \frac{\partial v_3}{\partial l} = \frac{\partial v_3}{L \partial s} \qquad \text{at } s = 0, 0.5, 1 \tag{4.28}$$

Taking the tangential component of angular velocity at mid-side node equal to the average angular velocity of the end nodes such as:

$$w_s^6 = \frac{\left(w_s^1 + w_s^2\right)}{2} \tag{4.29}$$

A transformation procedure is introduced because of the orientation of the element (Figure 17).

$$\hat{e}_n = \hat{e}_1 \sin\alpha - \hat{e}_2 \cos\alpha$$

$$\sin\alpha = \frac{\left(y^2 - y^1\right)}{L} \tag{4.30}$$

$$\cos\alpha = \frac{\left(x^2 - x^1\right)}{L}$$

By inserting Equation (4.30) into (4.28), angular velocities of the mid sides can be eliminated from the unknowns. Therefore the quadratic interpolations for the angular velocities can be condensed as:

$$w_1 = \sum_{j=1}^{6} \omega_1^j \psi_j(\zeta,\eta) = \sum_{k=1}^{9}\sum_{j=1}^{6} \beta_k H_1^{kj} \Phi_j$$

$$w_2 = \sum_{j=1}^{6} \omega_2^j \psi_j(\zeta,\eta) = \sum_{k=1}^{9}\sum_{j=1}^{6} \beta_k H_2^{kj} \Phi_j \tag{4.31}$$

where Φ and β are defined as:

$$\Phi^T = \begin{bmatrix} \varphi_1 & \varphi_2 & \varphi_3 & \psi_4 & \psi_5 & \psi_6 \end{bmatrix}$$
$$\beta = \begin{bmatrix} w_1^1 & w_1^2 & w_1^3 & w_2^1 & w_2^2 & w_2^3 & v_3^1 & v_3^2 & v_3^3 \end{bmatrix} \tag{4.32}$$

Explicit form of the H_1 and H_2 matrices can be found in the following equations:

$$H_1 = \begin{bmatrix} 1 & 0 & 0 & 0 & -ss(a_2) & -ss(a_3) \\ 0 & 1 & 0 & -ss(a_1) & 0 & -ss(a_3) \\ 0 & 0 & 1 & -ss(a_1) & -ss(a_2) & 0 \\ 0 & 0 & 0 & 0 & sc(a_2) & sc(a_3) \\ 0 & 0 & 0 & sc(a_1) & 0 & sc(a_3) \\ 0 & 0 & 0 & sc(a_1) & sc(a_2) & 0 \\ 0 & 0 & 0 & 0 & sl(a_2,l_2) & -sl(a_3,l_3) \\ 0 & 0 & 0 & -sl(a_1,l_1) & 0 & sl(a_3,l_3) \\ 0 & 0 & 0 & sl(a_1,l_1) & -sl(a_2,l_2) & 0 \end{bmatrix} \tag{4.33}$$

$$H_2 = \begin{bmatrix} 1 & 0 & 0 & 0 & sc(a_2) & sc(a_3) \\ 0 & 1 & 0 & sc(a_1) & 0 & sc(a_3) \\ 0 & 0 & 1 & sc(a_1) & sc(a_2) & 0 \\ 0 & 0 & 0 & 0 & -cc(a_2) & -cc(a_3) \\ 0 & 0 & 0 & -cc(a_1) & 0 & -cc(a_3) \\ 0 & 0 & 0 & -cc(a_1) & -cc(a_2) & 0 \\ 0 & 0 & 0 & 0 & -cl(a_2,l_2) & cl(a_3,l_3) \\ 0 & 0 & 0 & cl(a_1,l_1) & 0 & -cl(a_3,l_3) \\ 0 & 0 & 0 & -cl(a_1,l_1) & cl(a_2,l_2) & 0 \end{bmatrix} \tag{4.34}$$

where a_i is the angle between the i[th] side of the triangle and axis; l_i is the length of i[th] side. Other expressions in Equations (4.33) and (4.34) are defined as follows:

$$
\begin{aligned}
ss(a_i) &= 0.75\sin(a_i)\sin(a_i) \\
sc(a_i) &= 0.75\sin(a_i)\cos(a_i) \\
cc(a_i) &= 0.75\cos(a_i)\cos(a_i) \\
sl(a_i, l_i) &= 1.5\sin(a_i)/l_i \\
cl(a_i, l_i) &= 1.5\cos(a_i)/l_i
\end{aligned}
\tag{4.35}
$$

To sum up, velocities can be expressed in terms of nodal degrees of freedoms as:

$$
\begin{bmatrix} V_1 \\ V_2 \\ V_3 \\ W_1 \\ W_2 \end{bmatrix} = [N]_{5x15} \begin{bmatrix} v_1^1 & v_2^1 & v_3^1 & w_1^1 & w_2^1 & v_1^2 & v_2^2 & v_3^2 & w_1^2 & w_2^2 & v_1^3 & v_2^3 & v_3^3 & w_1^3 & w_2^3 \end{bmatrix}^T \tag{4.36}
$$

The total shape function *"N"* can be expressed in terms of natural and area coordinates as follows:

$$N^T = \begin{bmatrix} 1-\xi-\eta & 0 & 0 & 0 & 0 \\ 0 & 1-\xi-\eta & 0 & 0 & 0 \\ 0 & 0 & N_{11} & N_{12} & N_{13} \\ 0 & 0 & N_{21} & N_{22} & N_{23} \\ 0 & 0 & N_{31} & N_{32} & N_{33} \\ \xi & 0 & 0 & 0 & 0 \\ 0 & \xi & 0 & 0 & 0 \\ 0 & 0 & N_{41} & N_{42} & N_{43} \\ 0 & 0 & N_{51} & N_{52} & N_{53} \\ 0 & 0 & N_{61} & N_{62} & N_{63} \\ \eta & 0 & 0 & 0 & 0 \\ 0 & \eta & 0 & 0 & 0 \\ 0 & 0 & N_{71} & N_{72} & N_{73} \\ 0 & 0 & N_{81} & N_{82} & N_{83} \\ 0 & 0 & N_{91} & N_{92} & N_{93} \end{bmatrix} \tag{4.37}$$

where N_{ij} is defined as follows:

$$\begin{aligned} N_{11} &= \zeta_1^2\left(3-2\zeta_1\right)+2\zeta_1\zeta_2\zeta_3 \\ N_{21} &= \zeta_1^2\left(y_{12}\zeta_2-y_{31}\zeta_3\right)+\left(y_{12}-y_{31}\right)\zeta_1\zeta_2\zeta_3 \\ N_{31} &= \zeta_1^2\left(x_{21}\zeta_2-x_{13}\zeta_3\right)+\left(x_{21}-x_{13}\right)\zeta_1\zeta_2\zeta_3 \\ N_{41} &= \zeta_2^2\left(3-2\zeta_2\right)+2\zeta_1\zeta_2\zeta_3 \\ N_{51} &= \zeta_2^2\left(y_{23}\zeta_3-y_{12}\zeta_1\right)+\left(y_{23}-y_{12}\right)\zeta_1\zeta_2\zeta_3 \\ N_{61} &= \zeta_2^2\left(x_{32}\zeta_3-x_{21}\zeta_1\right)+\left(x_{32}-x_{21}\right)\zeta_1\zeta_2\zeta_3 \\ N_{71} &= \zeta_3^2\left(3-2\zeta_3\right)+2\zeta_1\zeta_2\zeta_3 \\ N_{81} &= \zeta_3^2\left(y_{31}\zeta_1-y_{23}\zeta_2\right)+\left(y_{31}-y_{23}\right)\zeta_1\zeta_2\zeta_3 \\ N_{91} &= \zeta_3^2\left(x_{13}\zeta_1-x_{32}\zeta_2\right)+\left(x_{13}-x_{32}\right)\zeta_1\zeta_2\zeta_3 \end{aligned} \tag{4.38}$$

$$
\begin{aligned}
N_{21} &= \eta - 3\eta(1-\xi-\eta)\sin^2(a_2) - 3\xi\eta\sin^2(a_1) \\
N_{22} &= 1-\xi-\eta - 3\eta(1-\xi-\eta)\sin^2(a_2) - 3\xi(1-\xi-\eta)\sin^2(a_3) \\
N_{23} &= \xi - 3\zeta(1-\xi-\eta)\sin^2(a_3) - 3\xi\eta\sin^2(a_1) \\
N_{24} &= 3\eta(1-\xi-\eta)\sin(a_2)\cos(a_2) + 3\xi\eta\sin(a_1)\cos(a_1) \\
N_{25} &= 3(1-\xi-\eta)\left[\eta\sin(a_2)\cos(a_2) + \xi\sin^2(a_3)\right] \\
N_{26} &= 3\xi(1-\xi-\eta)\sin(a_3)\cos(a_3) + 3\xi\eta\sin(a_1)\cos(a_1) \\
N_{27} &= 6\eta(1-\xi-\eta)\sin(a_2)/l_2 + 6\eta\xi\sin(a_1)/l_1 \\
N_{28} &= 6(1-\xi-\eta)\left[\left(\eta\sin(a_2)/l_2\right) - \left(\xi\sin(a_3)/l_3\right)\right] \\
N_{29} &= 6\xi(1-\xi-\eta)\sin(a_3)/l_3 - 6\eta\xi\sin(a_1)/l_1
\end{aligned}
\tag{4.39}
$$

$$
\begin{aligned}
N_{31} &= \eta - 3\eta(1-\xi-\eta)\sin(a_2)\cos(a_2) + 3\xi\eta\sin(a_1)\cos(a_1) \\
N_{32} &= 1-\xi-\eta - 3\eta(1-\xi-\eta)\cos(a_2)\sin(a_2) - 3\xi(1-\xi-\eta)\sin(a_3)\cos(a_3) \\
N_{33} &= \xi + 3\xi(1-\xi-\eta)\sin(a_3)\cos(a_3) + 3\xi\eta\sin(a_1)\cos(a_1) \\
N_{34} &= 3\eta(1-\xi-\eta)\cos^2(a_2) + 3\xi\eta\cos^2(a_1) \\
N_{35} &= 3(1-\xi-\eta)\left[\eta\cos^2(a_2) + \xi\cos^2(a_3)\right] \\
N_{36} &= 3\xi(1-\xi-\eta)\cos^2(a_3) + 3\xi\eta\cos^2(a_1) \\
N_{37} &= 6\eta(1-\xi-\eta)\cos(a_2)/l_2 + 6\eta\xi\cos(a_1)/l_1 \\
N_{38} &= 6(1-\xi-\eta)\left[\left(\eta\cos(a_2)/l_2\right) - \left(\xi\cos(a_3)/l_3\right)\right] \\
N_{39} &= 6\xi(1-\xi-\eta)\cos(a_3)/l_3 - 6\eta\xi\cos(a_1)/l_1
\end{aligned}
\tag{4.40}
$$

For calculating internal force vectors, one point quadrature for membrane part and 2 or more point quadrature for bending part are adapted. Therefore internal force vectors can be calculated by taking the following integrals [***42***]:

$$
\begin{aligned}
f_{xI} &= \int_V \left(B_{1I}\sigma_x + B_{2I}\sigma_{xy} \right) dV \\
f_{yI} &= \int_V \left(B_{2I}\sigma_y + B_{1I}\sigma_{xy} \right) dV \\
f_{zI} &= \int_V \left(B_{1I}\sigma_{xz} + B_{2I}\sigma_{yz} \right) dV \\
m_{xI} &= -\int_V \left(B_{2I}\sigma_y z + B_{1I}\sigma_{xy} z + \Phi_I \sigma_{yz} \right) dV \\
m_{yI} &= \int_V \left(B_{1I}\sigma_x z + B_{2I}\sigma_{xy} z + \Phi_I \sigma_{xz} \right) dV
\end{aligned}
\tag{4.41}
$$

By referring to Equation (4.11), internal force vectors are sufficient to calculate stresses. Therefore no stiffness matrix formation is needed for the calculations.

4.6.1 Velocity Gradient

To express large deformations in dynamic transient problems velocity gradient is used [***25***]:

$$
L = \begin{bmatrix}
\frac{\partial v_1}{\partial X_1} & \frac{\partial v_1}{\partial X_2} & \frac{\partial v_1}{\partial X_3} \\
\frac{\partial v_2}{\partial X_1} & \frac{\partial v_2}{\partial X_2} & \frac{\partial v_2}{\partial X_3} \\
\frac{\partial v_3}{\partial X_1} & \frac{\partial v_3}{\partial X_2} & \frac{\partial v_3}{\partial X_3}
\end{bmatrix}
\tag{4.42}
$$

Velocity gradient can be decomposed into rate of deformation and spin tensors as follows:

$$
L = D + \Omega \tag{4.43}
$$

Rate of deformation (strain rate) can be defined in terms of deformation gradient as:

$$D = \dot{\varepsilon} = \frac{1}{2}\left(\dot{F}F^{-1} + F^{-T}\dot{F}^{T}\right) \tag{4.44}$$

The spin can be calculated as follows:

$$\Omega = \frac{1}{2}\left(\dot{F}F^{-1} - F^{-T}\dot{F}^{T}\right) \tag{4.45}$$

Therefore the rotation can be found from:

$$R = I + \Omega \tag{4.46}$$

where I is the identity matrix.

4.6.2 Jacobian Matrix

Jacobian matrix is used in terms of natural coordinates for the calculations which can be defined as:

$$\begin{bmatrix} \frac{\partial}{\partial \xi} \\ \frac{\partial}{\partial \eta} \\ \frac{\partial}{\partial \varsigma} \end{bmatrix} = \underbrace{\begin{bmatrix} \frac{\partial x}{\partial \xi} & \frac{\partial y}{\partial \xi} & \frac{\partial z}{\partial \xi} \\ \frac{\partial x}{\partial \eta} & \frac{\partial y}{\partial \eta} & \frac{\partial z}{\partial \eta} \\ \frac{\partial x}{\partial \varsigma} & \frac{\partial y}{\partial \varsigma} & \frac{\partial z}{\partial \varsigma} \end{bmatrix}}_{J} \begin{bmatrix} \frac{\partial}{\partial x} \\ \frac{\partial}{\partial y} \\ \frac{\partial}{\partial z} \end{bmatrix} \tag{4.47}$$

$$J = \begin{bmatrix} x_2 - x_3 & y_2 - y_1 \\ x_3 - x_1 & y_3 - y_1 \end{bmatrix} = \begin{bmatrix} \gamma_3 & -\beta_3 \\ -\gamma_2 & \beta_2 \end{bmatrix} \tag{4.48}$$

Inverse of the Jacobian can be obtained by using the following relation:

$$J^{-1} = \frac{1}{\det J}\begin{bmatrix} \beta_2 & \beta_3 \\ \gamma_2 & \gamma_3 \end{bmatrix} \tag{4.49}$$

4.6.3 Stress Update Procedure

The numerical algorithm for a single time step follows the procedure described below:

1- Calculate D and W

2- Compute

$$z_i = e_{ijk} D_{jm} V_{mk} \tag{4.50}$$

$$\omega = w + \left[IV^T - V \right]^{-1} z \tag{4.51}$$

$$\Omega_{ij} = e_{ikj} \omega_k \tag{4.52}$$

3- Calculate $R_{t+\Delta t}$

$$\left(I - \tfrac{1}{2} \Delta t \Omega \right) R_{t+\Delta t} = \left(I + \tfrac{1}{2} \Delta t \Omega \right) R_t \tag{4.53}$$

4- Calculate velocity gradient

$$L = \left(D + W \right) V - V \Omega \tag{4.54}$$

5- Update velocity

$$V_{t+\Delta t} = V_t + \Delta t \dot{V}_{\Delta t} \tag{4.55}$$

6- Compute

$$d = R^t D R \tag{4.56}$$

7- Integrate stress

$$\dot{\sigma} = f\left(d, \sigma\right) \tag{4.57}$$

8- Compute

$$T = R\sigma R^{t} \tag{4.58}$$

4.6.4 Plasticity for the Developed Code

In the case of yielding, application of the update algorithm is as follows [***26***]:

1- The stress σ is updated elastically.

2- Yield condition is checked:

$$f = \sqrt{3J_2} - \sigma_y$$
$$= \frac{1}{\sqrt{2}}\sqrt{\left(\sigma_{xx} - \sigma_{yy}\right)^2 + \left(\sigma_{yy} - \sigma_{zz}\right)^2 + \left(\sigma_{zz} - \sigma_{xx}\right)^2 + 6\left(\tau^2_{xy} + \tau^2_{yz} + \tau^2_{zx}\right)} - \sigma_y \tag{4.59}$$

3- If no yielding occurs ($f \leq 0$), stresses are calculated by elastic update as described in Section 3.2.3.

4- If stresses exceed the elastic limit (f > 0), plastic strain increment is evaluated as:

$$\Delta\varepsilon_{pl} = \frac{\sigma_{evm} - \sigma_y}{E_{plastic}} \tag{4.60}$$

5- Effective plastic strain ε_{eff} is updated as:

$$\varepsilon_{eff,pl}{}^{n+1} = \varepsilon_{eff,pl}{}^{n} + \Delta\varepsilon_{pl} \tag{4.61}$$

6- New flow stress is calculated as:

$$\sigma_y^{n+1} = \sigma_y^{n} + E_{pl}\Delta\varepsilon_{pl} \tag{4.62}$$

7- Proceed to next step

4.7 Mass Matrix for the Triangular Element

As stated in Section 3.6, lumped mass matrix of an element can be calculated by simply dividing the mass of the element into three:

$$[M] = \frac{1}{3}\rho A t \begin{bmatrix} 1 & & & & & \\ & 1 & & & & \\ & & 1 & & & \\ & & & \frac{t^2}{12} & & \\ & & & & \frac{t^2}{12} & \\ & & & & & \end{bmatrix} \tag{4.63}$$

4.8 Constitutive Relation

The constitutive relation for the shell element in three dimensions is as follows:

$$[C] = \frac{E(1-\nu)}{(1+\nu)(1-2\nu)} \begin{bmatrix} 1 & \frac{\nu}{1-\nu} & 0 & 0 & 0 \\ \frac{\nu}{1-\nu} & 1 & 0 & 0 & 0 \\ 0 & 0 & \frac{1-2\nu}{2(1-\nu)} & 0 & 0 \\ 0 & 0 & 0 & \frac{1-2\nu}{2(1-\nu)} & 0 \\ 0 & 0 & 0 & 0 & \frac{1-2\nu}{2(1-\nu)} \end{bmatrix} \tag{4.64}$$

If the flow stress is exceeded, C is replaced by C_p as described in Section 3.3.

4.9 Input Parameters and Solution Controls

Graphical user interface of the program is shown in Appendix A. Input and solution control parameters are entered through this user interface. These controls include:

- Elastic modulus
- Plastic modulus
- Poisson`s ratio
- Thickness of plate
- Density
- Number of through thickness integration points (≤ 5)
- Scale factor for critical timestep (recommended value: ≤0.9)
- Termination time
- Output interval
- Output node & element number

CHAPTER 5

RESULTS AND DISCUSSION

In this chapter, several benchmark studies are carried out in order to evaluate the performance of the developed code considering blast loading. Blast load input is taken in the form of pressure time history data. The results are compared with the experimental data taken from literature and simulation results of Ls-Dyna program. Six different experimental configurations are simulated. Furthermore parameter sensitivity study is carried out by means of mesh sensitivity, material model and number of through thickness integration points. After observing convergent and reliable results for the mentioned parameters for the first configuration, remaining configurations are simulated by using these parameters. The results of both programs are compared and discussed.

5.1 Experimental Data

In order to correlate the finite element simulation results a comparison with the experimental data is needed. The test data is taken from the original work of Neuberger et al. [***43***] which investigated dynamic behavior of Rolled Homogenous Armor (RHA) steel disks under blast loads. A spherical charge of TNT was detonated above the center point at a specified distance (Figure 18).

Maximum deformation is measured by using a comb-like device (Figure 19). Test configurations and results are summarized in Table 5.1.

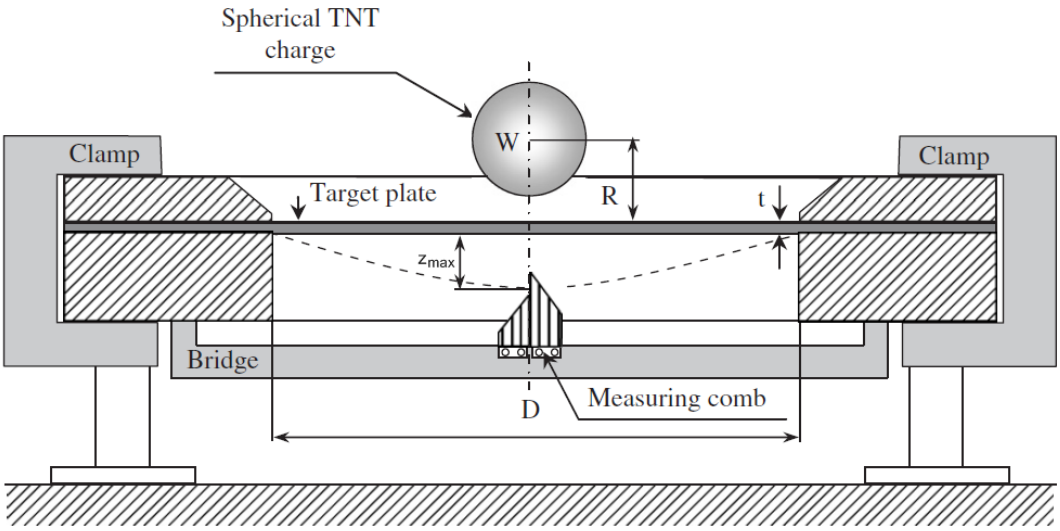

Figure 18: Schematic diagram of test setup [***43***]

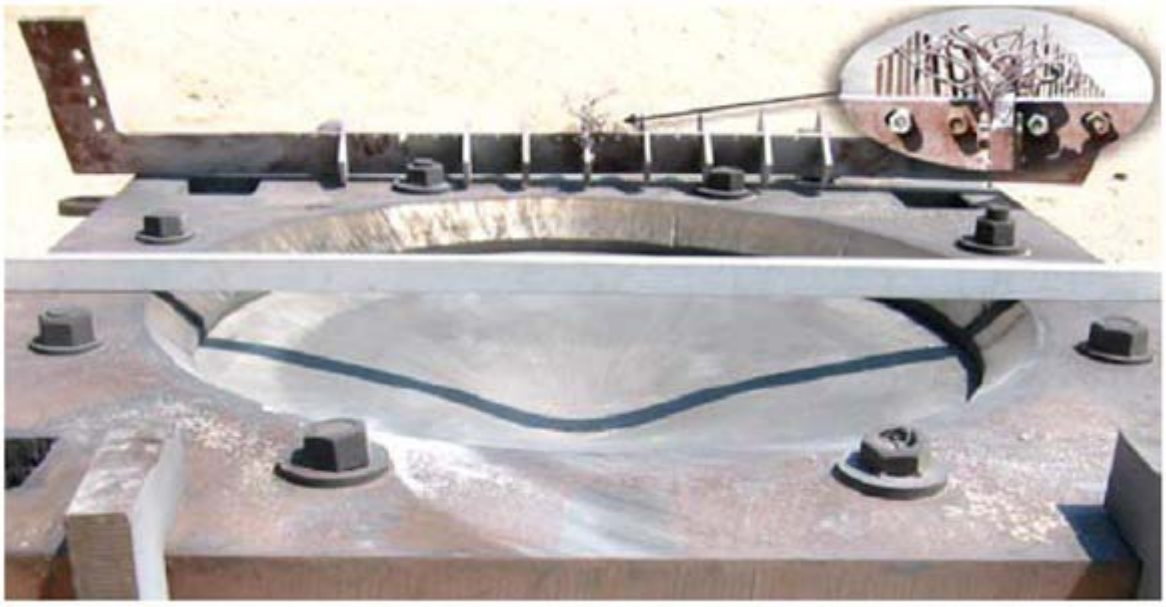

Figure 19: Permanent deformation of the plate and measuring comb [***43***]

Table 5.1: Configurations and results for the tests of Neuberger et al. [***43***]

Case No	Thickness (mm)	Diameter of RHA (mm)	TNT Mass (kg)	Distance of Charge (mm)	Maximum Deflection (mm)
1	20	1000	3.750	200	54
2	10	500	0.468	100	26
3	20	1000	8.750	200	107
4	10	500	1.094	100	48.5
5	20	1000	8.750	130	165
6	10	500	1.094	65	74.5

The material data is given by considering three different material models for the RHA plates used in the experiments. These are:

i. Johnson - Cook Material Model (Equation (3.27)) with Mie Gruneisen Equation of State (Equation (3.26))

ii. Cowper – Symonds Material Model (Equation (3.29))

iii. Bilinear Elastic Plastic Material Model (Figure 12)

The values used for the above material models are given in the following tables:

Table 5.2: Johnson-Cook material model constants for RHA [***43***]

Young`s Modulus	Yield Strength	Strain Hardening Constant	Strain Hardening Exponent	Strain Rate Constant
E (GPa)	**A (MPa)**	**B (MPa)**	**n (MPa)**	**C**
210	900	545	0.26	0.014

Table 5.3: Bilinear elastic-plastic material model constants for RHA [***43***]

Young`s Modulus E (GPa)	Plastic Modulus E_p (GPa)	Yield Strength σ_y (MPa)
210	2	1000

Table 5.4: Cowper - Symons material model constants for RHA [***43***]

Young`s Modulus E (GPa)	Yield Strength σ_y (MPa)	Plastic Modulus E_p (GPa)	Strain Rate Parameter $D^*(s^{-1})$	Strain Rate Parameter q
210	1200	6.5	300	5

5.2 Finite Element Simulations by a Commercial Code

Since the RHA plate is heavily clamped, it is assumed as fully constrained around the periphery (all degrees of freedom are fixed at the periphery). One fourth symmetric model is used for reducing the computational cost. Geometry and finite element mesh used in all 10 mm triangular element cases are presented in (Figure 20).

For all simulations blast load is determined by using the Ls-Dyna program as a function of time for each individual element. The default hourglass control method for shell elements (viscous form) is chosen for Ls-Dyna simulations.

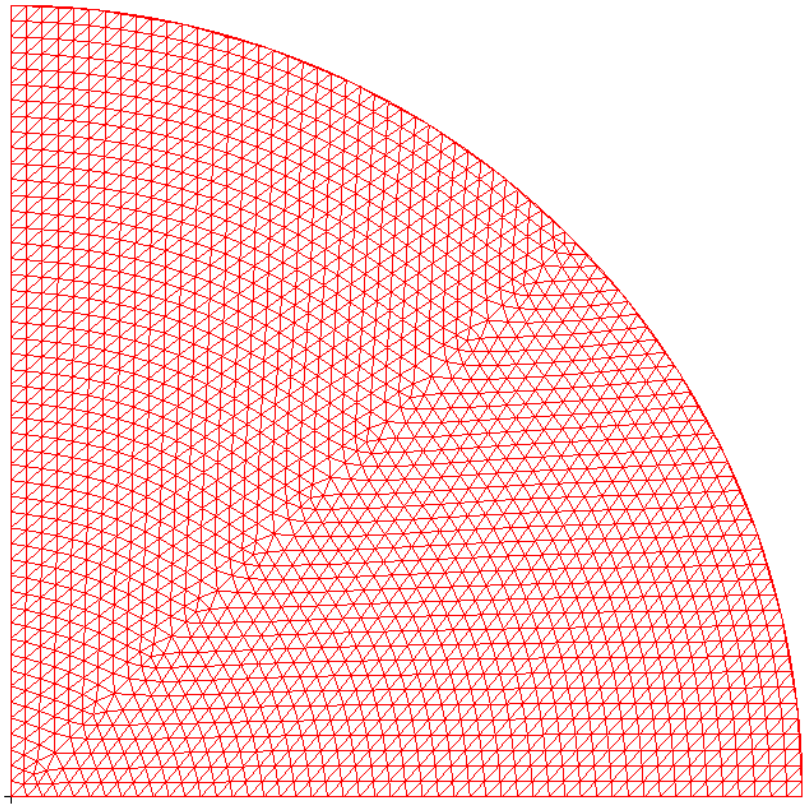

Figure 20: Finite element model used in the simulations

5.2.1 Case I

In this case, the first set-up of the experimental study (Table 5.1) is simulated. Plate thickness is taken as 20 mm with a diameter of 1000 mm. Total mass of TNT is 3.75 kg which is detonated at 200 mm distance to the midpoint of RHA plate. Maximum deformation is reported as 54 mm [***43***].

Finite element simulation performance can be affected by various factors such as material model, element type, mesh size and number of integration points (NIP) through the thickness of element. Thus a parameter sensitivity study must be conducted in order to investigate of these parameters on the results.

For Ls-Dyna simulations; parameter study is carried out for material model, element type, mesh size and number of integration points through the thickness of element. Detailed information about element types can be found in [***16***].

Calculated time of arrival for the blast wave is 34.98 micro seconds with a peak pressure of 278.47 MPa.

5.2.1.1 Parameter Study for Element Type

For simulations of Case I, 4 different element types are used:

1. Quadrilateral
2. Triangular (Collapsed Quad)
3. Triangular (Element Formulation 3)
4. Triangular (Element Formulation 4)

By default Ls-Dyna uses quadrilateral element treatment for shells. Triangular elements are treated as collapsed quad element if it is not specified otherwise.

Obtained results are summarized in Table 5.5 (NIP: Number of thorough thickness integration points, Z max: Maximum deflection of the RHA plate).

Table 5.5: Parameter study for element type

Elm Type	**Mesh (mm)**	**Material Model**	**NIP**	**Z max (mm)**	**TEST (mm)**	**Difference** (%)
Quad	10	Elastic Plastic	4	58.31	54.0	7.98
Tria				58.06		7.52
Tria – ELF3				66.00		22.23
Tria – ELF 4				58.30		7.97

Two sample deformed configurations with contours of z axis displacement are presented in the following figures:

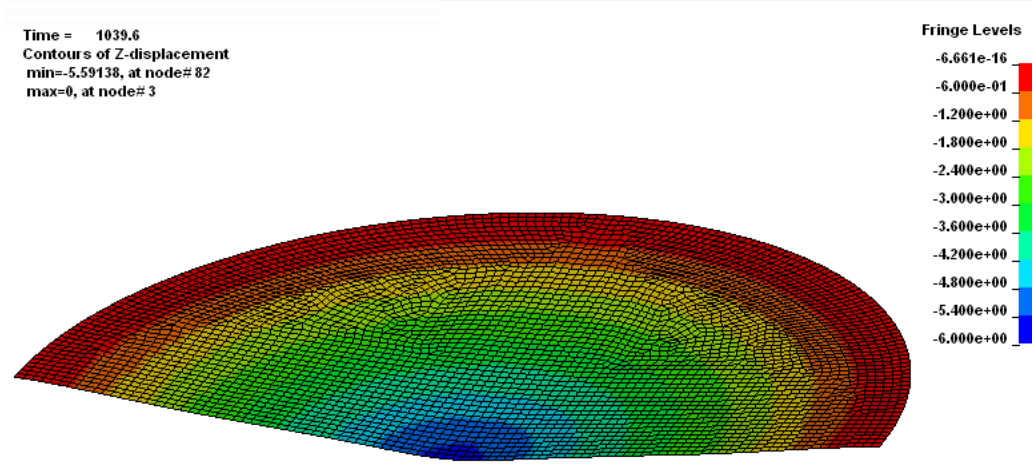

Figure 21: Deformation contour plot for 10 mm quad mesh with Elastic – Plastic material model and 4 through thickness integration points

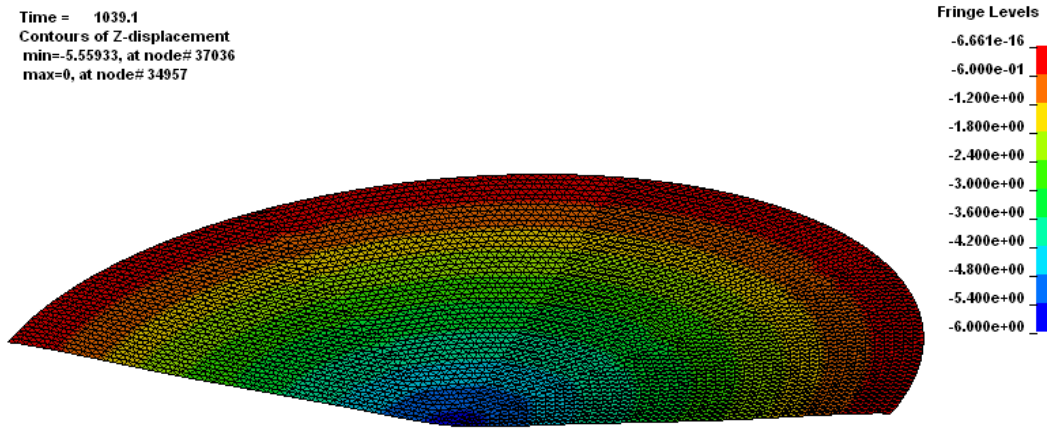

Figure 22: Deformation contour plot for 10 mm triangular mesh with Elastic – Plastic material model and 4 through thickness integration points

When the obtained results are discussed, it is concluded that default quadrilateral, collapsed quadrilateral and triangular element with formulation option 4 are suitable for this kind of study. Since this thesis study focuses on triangular elements, best performing triangular element is chosen to be with the 4^{th} formulation option according to Table 5.5.

5.2.1.2 Parameter Study for Mesh Size

Effect of mesh size on the results is investigated by using triangular element with 4th formulation as summarized in Table 5.6.

Table 5.6: Parameter study for mesh size

Elm Type	Mesh (mm)	Material Model	NIP	Z max (mm)	TEST (mm)	Difference (%)
Tria - ELF 4	5	Elastic Plastic	3	58.3	54	8.03
	10			58.3		7.97
	20			58.3		7.61

Mesh sensitivity study gave very close results for 5, 10 and 20 mm element sizes. Thus 10 mm is preferred for the remaining study from the point of accuracy and computational cost.

5.2.1.3 Parameter Study for Material Model

Three different material models are used including Elastic – Plastic, Johnson Cook and Cowper Symonds while keeping other parameters constant. Comparison of the parameter sensitivity study for material model is summarized in the following table for triangular element (4th formulation) with 10 mm mesh size and 4 integration points through thickness:

Table 5.7: Parameter study for material models

Elm Type	Mesh (mm)	Material Model	NIP	Z max (mm)	TEST (mm)	Difference (%)
Tria – ELF4	10	Elastic Plastic	4	58.3	54	7.97
		Johnson Cook + Shock	4	56.92		5.41
		Cowper Symonds	4	42.28		21.7

When the results are investigated it is observed that, Elastic - Plastic and Johnson Cook material models can capture the deformation behavior in good agreement with the test results. On the other hand, Cowper Symonds model gave relatively higher differences.

5.2.1.4 Parameter Study for Number of Integration Points

Another important parameter is the number of integration points through the element thickness which has influence on transverse shear and bending behavior of the element. Parameter study is conducted by using 10 mm triangular elements with elastic plastic material model. The results are summarized in Table 5.8.

Results of this study showed that even one integration point seems to give closer results; main issue is not to “shoot” the real data but to obtain a stable and repeatable result. A generic example is presented in Figure 23. The closest result seems to happen when number of integration points is equal to 1. However for repeatability and stability of the solution, the results must be independent of that parameter, therefore 4 integration points will be more appropriate.

Table 5.8: Parameter study for number of through thickness integration points

Elm Type	Mesh (mm)	MAT	NIP	Z max (mm)	TEST (mm)	Difference (%)
Tria	10	Elastic Plastic	1	56.04	54	3.78
			2	60.9		12.78
			3	55.8		3.33
			4	58.06		7.52
			5	5.82		7.78
			6	5.723		5.98

Because of the points mentioned above, 4 integration points appear most applicable in terms of accuracy and efficiency.

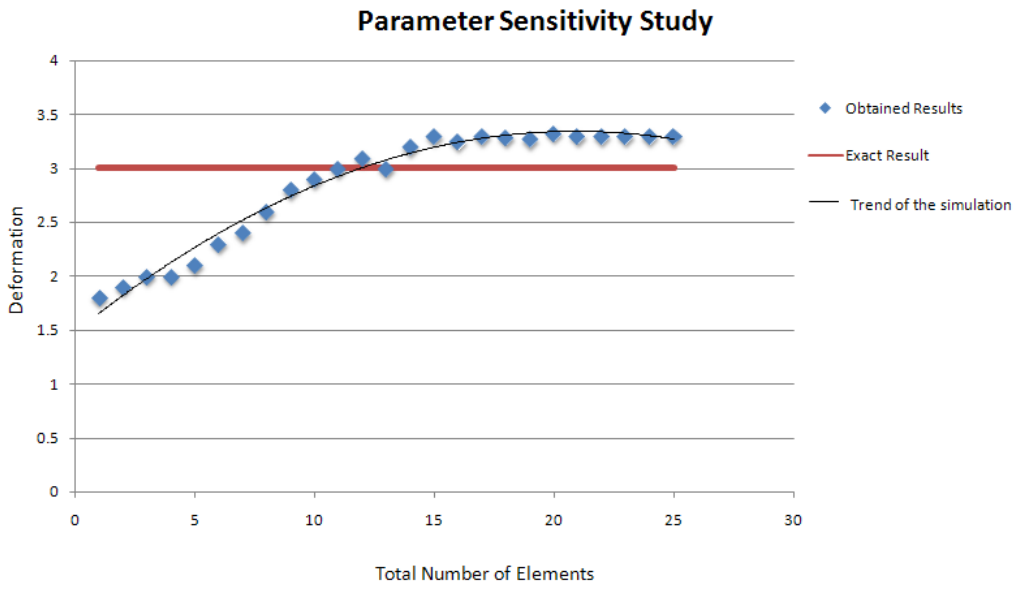

Figure 23: Generic simulation trend and an exact result

5.2.2 Case 2

In this case, the second set up of the experimental study (Table 5.1) is simulated. Plate thickness is taken as 10 mm with a diameter of 500 mm. Total mass of TNT is 468 g which is detonated at 100 mm distance to the midpoint of RHA plate. Maximum deformation is reported as 26 mm [***43***].

As the parameter sensitivity study is carried out in the previous section, finite element simulation will be done by fixed model parameters for the rest of configurations. The only reported variable for the tests is maximum deflection. Thus results of the finite element study are verified for the displacement regarding configuration 1.

For Ls-Dyna simulation, 10 mm triangular element with 4^{th} formulation is selected. 4 through thickness integration points are assigned. Time of arrival of the blast wave is 17.40 microseconds with a pressure of 278.65 MPa. Maximum deformation occurs around 730 microseconds. Result of the simulation is presented in Table 5.9:

Table 5.9: Maximum deformation for Case 2 (Ls-Dyna simulation)

Elm Type	Mesh mm	MAT	NIP	Z max (mm)	Test (mm)	Difference (%)
Tria - ELF 4	10	Elastic Plastic	4	29.07	26.0	11.81

5.2.3 Case 3

In this case, the third set up of the experimental study (Table 5.1) is simulated. Plate thickness is taken as 20 mm with a diameter of 1000 mm. Total mass of TNT is 8.75 kg which is detonated at 200 mm distance to the midpoint of RHA

plate. Maximum deformation is reported as 107 mm [***43***]. Result of the simulation is presented in Table 5.9:

Table 5.10: Maximum deformation for Case 3 (Ls-Dyna simulation)

Elm Type	Mesh mm	MAT	NIP	Z max (mm)	Test (mm)	Difference (%)
Tria - ELF 4	10	Elastic Plastic	4	131.67	107.0	23.06

5.2.4 Case 4

In this case, the fourth set up of the experimental study (Table 5.1) is simulated. Plate thickness is taken as 10 mm with a diameter of 500 mm. Total mass of TNT is 1.09 kg which is detonated at 100 mm distance to the midpoint of RHA plate. Maximum deformation is reported as 48.5 mm [***43***]. Result of the simulation is presented in Table 5.9:

Table 5.11: Maximum deformation for Case 4 (Ls-Dyna simulation)

Elm Type	Mesh mm	MAT	NIP	Z max (mm)	Test (mm)	Difference (%)
Tria - ELF 4	10	Elastic Plastic	4	61.57	48.5	26.95

5.2.5 Case 5

In this case, the fifth set up of the experimental study (Table 5.1) is simulated. Plate thickness is taken as 20 mm with a diameter of 1000 mm. Total mass of

TNT is 8.75 kg which is detonated at 130 mm distance to the midpoint of RHA plate. Maximum deformation is reported as 165 mm [***43***]. Result of the simulation is presented in Table 5.9:

Table 5.12: Maximum deformation for Case 5 (Ls-Dyna simulation)

Elm Type	Mesh mm	MAT	NIP	Z max (mm)	Test (mm)	Difference (%)
Tria - ELF 4	10	Elastic Plastic	4	168.47	165.0	2.07

5.2.6 Case 6

In this case, the sixth set up of the experimental study (Table 5.1) is simulated. Plate thickness is taken as 10 mm with a diameter of 500 mm. Total mass of TNT is 1.094 kg which is detonated at 65 mm distance to the midpoint of RHA plate. Maximum deformation is reported as 74.5 mm [***43***]. Result of the simulation is presented in Table 5.9:

Table 5.13: Maximum deformation for Case 6 (Ls-Dyna simulation)

Elm Type	Mesh mm	MAT	NIP	Z max (mm)	Test (mm)	Difference (%)
Tria - ELF 4	10	Elastic Plastic	4	84.22	74.5	13.05

5.3 Developed Code Simulations

Since the developed code uses a pre defined element formulation and material model, parameter study is carried out for mesh size and number of integration points through the thickness.

5.3.1 Case I

The experimental set up is the same as in the Ls-Dyna simulations (5.2.1). Also the same finite element model is used (Figure 20) for compatibility of pressure data. Since the material model and element type is fixed in the developed code, parameter study is carried out mesh size and number of integration points.

5.3.1.1 Parameter Study for Mesh Size

Sensitivity study results for element size parameter are summarized in Table 5.14. The results showed that 5, 10 and 20 mm meshes give very close results as in the case of Ls-Dyna simulations. Therefore 10 mm mesh size is chosen as an optimum value.

Table 5.14: Parameter study for element size

Element	Mesh mm	MAT	NIP	Z max (mm)	Test (mm)	Difference (%)
Developed Code	5	Elastic Plastic	4	58.34	54.0	8,84
	10			58.35		8.05
	20			58.20		7.78

5.3.1.2 Parameter Study for Integration Points

The developed code allows up to 5 integration points through the thickness. Therefore effect of number of integration points is also investigated. Obtained

results are listed in Table 5.15. It shows that for a converged result 4 integration points can be chosen.

According to the results of integration point sensitivity study, it is concluded that 4 integration points in the thickness is appropriate for converged and stable deformation behavior.

Table 5.15: Parameter study for element number of integration points

Elm Type	Mesh (mm)	MAT	NIP	Z max (mm)	Test (mm)	Difference (%)
Developed Code	10	Elastic Plastic	1	54.00	54.0	0.00
			2	61.29		13.50
			3	56.00		3.70
			4	58.35		8.05
			5	58.51		8.35

5.3.2 Case 2

Details of the second experimental configuration are presented in Section 5.2.2.

As the parameter sensitivity study is carried out in the previous section, finite element simulation will be done by fixed model parameters for the second configuration.

For developed code simulations, 10 mm triangular element with 4 integration points is selected. The same finite element mesh is used for the developed code and Ls-Dyna. Maximum deformation value of the simulation is given in Table 5.16.

Table 5.16: Maximum deformation for Case 2 (Developed code simulation)

Elm Type	Mesh mm	MAT	NIP	Z max (mm)	Test (mm)	Difference (%)
Developed Code	10	Elastic Plastic	4	29.10	26.0	11.92

5.3.3 Case 3

Details of the second experimental configuration are presented in Section 5.2.3. Maximum deformation value of the simulation is given in Table 5.17.

Table 5.17: Maximum deformation for Case 3 (Developed code simulation)

Elm Type	Mesh mm	MAT	NIP	Z max (mm)	Test (mm)	Difference (%)
Tria - ELF 4	10	Elastic Plastic	4	131.69	107.0	23.07

5.3.4 Case 4

Details of the second experimental configuration are presented in Section 5.2.4. Maximum deformation value of the simulation is given in Table 5.18.

Table 5.18: Maximum deformation for Case 4 (Developed code simulation)

Elm Type	Mesh mm	MAT	NIP	Z max (mm)	Test (mm)	Difference (%)
Tria - ELF 4	10	Elastic Plastic	4	61.59	48.5	27.00

5.3.5 Case 5

Details of the second experimental configuration are presented in Section 5.2.5. Maximum deformation value of the simulation is given in Table 5.19.

Table 5.19: Maximum deformation for Case 5 (Developed code simulation)

Elm Type	Mesh mm	MAT	NIP	Z max (mm)	Test (mm)	Difference (%)
Tria - ELF 4	10	Elastic Plastic	4	168.37	165.0	2.04

5.3.6 Case 6

Details of the second experimental configuration are presented in Section 5.2.6. Maximum deformation value of the simulation is given in Table 5.20.

Table 5.20: Maximum deformation for Case 6 (Developed code simulation)

Elm Type	Mesh mm	MAT	NIP	Z max (mm)	Test (mm)	Difference (%)
Tria - ELF 4	10	Elastic Plastic	4	84.20	74.5	13.02

5.4 Comparison of Results

In this section, overall results of the finite element simulations and previous experimental data are compared.

5.4.1 Case 1

Finite element simulation results are compared with the experimental data for the first experimental case as follows:

Table 5.21: Comparison of maximum deformation results for Case 1

Code	Elm Type	Mesh (mm)	MAT	NIP	Z max (mm)	Test (mm)	Difference (%)
Developed Code	Tria	5	Elastic Plastic	4	58.34	54.0	8.04
	Tria	10	Elastic Plastic	4	58.35		8.05
	Tria	20	Elastic Plastic	4	58.20		7.78
	Tria	10	Elastic Plastic	1	54.00		0.00
	Tria	10	Elastic Plastic	2	61.29		13.50
	Tria	10	Elastic Plastic	3	56.00		3.70
	Tria	10	Elastic Plastic	5	58.51		8.35
Ls-Dyna	Quad	10	Elastic Plastic	5	58.41	54.0	8.17
	Quad	10	Johnson Cook	5	56.98		5.52
	Quad	10	Elastic Plastic	1	54.00		0.00
	Quad	10	Elastic Plastic	2	61.15		13.24
	Quad	10	Elastic Plastic	3	55.98		3.66
	Quad	10	Elastic Plastic	4	58.31		7.98
	Quad	10	Elastic Plastic	10	58.09		7.56
	Quad	5	Elastic Plastic	10	58.17		7.72
	Quad	5	Elastic Plastic	4	58.41		8.17
	Tria	10	Elastic Plastic	4	58.06		7.52
	Tria	5	Elastic Plastic	4	58.26		7.89
	Tria	10	Johnson Cook	4	56.92		5.41
	Tria	10	Cowper Symons	4	42.28		21.70
	Tria	10	Cowper Symons	5	56.67		4.94
	Tria	10	Elastic Plastic	1	56.04		3.78
	Tria	10	Elastic Plastic	2	60.90		12.78
	Tria	10	Elastic Plastic	3	55.80		3.33
	Tria	10	Elastic Plastic	4	58.06		7.52
	Tria	10	Elastic Plastic	5	58.20		7.78
	Tria	10	Elastic Plastic	6	57.23		5.98
	Tria - ELF 3	10	Elastic Plastic	4	66.00		22.23
	Tria - ELF 3	20	Elastic Plastic	4	57.84		7.11
	Tria - ELF 4	5	Elastic Plastic	4	58.34		8.03
	Tria - ELF 4	10	Elastic Plastic	4	58.30		7.97
	Tria - ELF 4	20	Elastic Plastic	4	58.11		7.61

After the comparison of overall results for the first experimental configuration, it is decided to use 10 mm triangular elements with 4th element formulation option for Ls-Dyna and 10 mm elements for the developed code simulations. Since finite element simulations with both Ls-Dyna and the developed code are validated for the first experimental case, results of the two programs can be compared directly. For this purpose, five different points are taken with 100 mm interval from the centerline of the plate. Comparison of maximum deformation, Von Mises stress and effective plastic strain is given below. When the results of two programs are investigated it can be concluded that they gave very close results.

Table 5.22: Comparison of maximum deformation results for Case 1

	R(0)	**R(100)**	**R(200)**	**R(300)**	**R(400)**
			Displacement (mm)		
Ls-Dyna	58.30	47.93	36.59	25.11	11.16
Developed Code	58.35	47.94	36.67	25.22	11.25
Difference (mm)	0.05	0.01	0.08	0.11	0.09
			Equivalent Von Mises Stress (MPa)		
Ls-Dyna	1146.63	1018.64	976.96	341.25	333.38
Developed Code	1217.86	1023.44	1000.09	348.87	339.53
Difference (MPa)	71.23	4.80	23.13	7.62	6.15
			Effective Plastic Strain (%)		
Ls-Dyna	12.61	3.13	1.41	0.91	0.01
Developed Code	13.28	3.33	1.52	0.94	0.01
Difference	0.67	0.20	0.11	0.03	0.00

5.4.2 Case 2

Results of the finite element simulations are compared with the experimental data in the following table:

Table 5.23: Comparison of maximum deformation results for Case 2

Program	Elm Type	Mesh (mm)	MAT	NIP	Z max (mm)	Test (mm)	Difference (%)
Ls-Dyna	Tria - ELF 4	10	Elastic Plastic	4	29.07	26.0	11.81
Developed Code	Tria				29.10		11.92

Five different points are taken with 50 mm interval from the centerline of the plate. Comparison of maximum deformation, Von Mises stress and effective plastic strain is given below.

Table 5.24: Comparison of simulation results at different locations for Case 2

	R(0)	R(50)	R(100)	R(150)	R(200)
	Displacement (mm)				
Ls-Dyna	29.07	23.90	18.25	12.53	5.57
Developed Code	29.10	23.90	18.30	12.59	5.62
Difference (mm)	0.03	0.00	0.05	0.06	0.05

	Equivalent Von Mises Stress (MPa)				
Ls-Dyna	1217.14	1045.58	1022.83	1018.49	1018.30
Developed Code	1208.28	1042.34	998.69	975.25	937.71
Difference (MPa)	8.86	3.24	24.14	43.24	80.59
	Effective Plastic Strain (%)				
Ls-Dyna	13.23	3.31	1.50	0.94	0.94
Developed Code	13.13	3.30	1.47	0.90	0.86
Difference	0.10	0.01	0.03	0.04	0.08

5.4.3 Case 3

Results of the finite element simulations are compared with the experimental data in the following table:

Table 5.25: Comparison of maximum deformation results for Case 3

Program	Elm Type	Mesh (mm)	MAT	NIP	Z max (mm)	Test (mm)	Difference (%)
Ls-Dyna	Tria - ELF 4	10	Elastic Plastic	4	131.67	107.0	23.06
Developed Code	Tria				131.69		23.07

Five different points are taken with 100 mm interval from the centerline of the plate. Comparison of maximum deformation, Von Mises stress and effective plastic strain is given below.

Table 5.26: Comparison of simulation results at different locations for Case 3

	R(0)	R(100)	R(200)	R(300)	R(400)
			Displacement (mm)		
Ls-Dyna	131.67	117.37	81.45	41.16	12.52
Developed Code	131.69	117.40	81.50	41.19	12.52
Difference (mm)	0.02	0.03	0.05	0.03	0.00
			Equivalent Von Mises Stress (MPa)		
Ls-Dyna	1402.40	1193.18	560.48	446.89	350.37
Developed Code	1400.27	1051.28	467.47	397.72	284.50
Difference (MPa)	2.13	141.90	93.01	49.17	65.87
			Effective Plastic Strain (%)		
Ls-Dyna	20.88	17.01	10.01	2.60	0.00
Developed Code	20.85	16.97	9.95	2.58	0.00
Difference	0.03	0.04	0.06	0.02	0.00

5.4.4 Case 4

Results of the finite element simulations are compared with the experimental data in the following table:

Table 5.27: Comparison of maximum deformation results for Case 4

Program	Elm Type	Mesh (mm)	MAT	NIP	Z max (mm)	Test (mm)	Difference (%)
Ls-Dyna	Tria - ELF 4	10	Elastic Plastic	4	61.57	48.5	26.95
Developed Code	Tria				61.59		27.00

Five different points are taken with 50 mm interval from the centerline of the plate. Comparison of maximum deformation, Von Mises stress and effective plastic strain is given below.

Table 5.28: Comparison of simulation results at different locations for Case 4

	R(0)	R(50)	R(100)	R(150)	R(200)
			Displacement (mm)		
Ls-Dyna	61.57	53.07	32.62	13.23	3.08
Developed Code	61.59	53.08	32.62	13.29	3.07
Difference (mm)	0.02	0.01	0.00	0.06	0.01
			Equivalent Von Mises Stress (MPa)		
Ls-Dyna	1399.11	1163.59	446.91	337.19	258.48
Developed Code	1394.57	1161.40	446.91	321.90	250.09
Difference (MPa)	4.54	2.19	0.00	15.29	8.39
			Effective Plastic Strain (%)		
Ls-Dyna	19.77	17.02	8.56	0.62	0.00
Developed Code	19.70	16.98	8.56	0.59	0.00
Difference	0.07	0.04	0.00	0.03	0.00

5.4.5 Case 5

Results of the finite element simulations are compared with the experimental data in the following table:

Table 5.29: Comparison of maximum deformation results for Case 5

Program	Elm Type	Mesh (mm)	MAT	NIP	Z max (mm)	Test (mm)	Difference (%)
Ls-Dyna	Tria - ELF 4	10	Elastic Plastic	4	168.42	165.0	2.07
Developed Code	Tria				168.37		2.04

Five different points are taken with 50 mm interval from the centerline of the plate. Comparison of maximum deformation, Von Mises stress and effective plastic strain is given below.

Table 5.30: Comparison of simulation results at different locations for Case 5

	R(0)	R(100)	R(200)	R(300)	R(400)
			Displacement (mm)		
Ls-Dyna	168.42	152.13	116.31	81.41	41.17
Developed Code	168.37	152.10	116.30	81.46	41.23
Difference (mm)	0.05	0.03	0.01	0.05	0.06
			Equivalent Von Mises Stress (MPa)		
Ls-Dyna	1446.12	1396.48	1286.92	1169.33	1123.47
Developed Code	1441.83	1284.76	1261.18	1134.25	1067.30
Difference (MPa)	4.29	111.72	25.74	35.08	56.17
			Effective Plastic Strain (%)		
Ls-Dyna	18.09	7.78	0.40	0.00	0.00
Developed Code	17.03	7.39	0.38	0.00	0.00
Difference	1.06	0.39	0.02	0.00	0.00

5.4.6 Case 6

Results of the finite element simulations are compared with the experimental data in the following table:

Table 5.31: Comparison of maximum deformation results for Case 6

Program	Elm Type	Mesh (mm)	MAT	NIP	Z max (mm)	Test (mm)	Difference (%)
Ls-Dyna	Tria - ELF 4	10	Elastic Plastic	4	84.22	74.5	13.05
Developed Code	Tria				84.20		13.02

Five different points are taken with 50 mm interval from the centerline of the plate. Comparison of maximum deformation, Von Mises stress and effective plastic strain is given below.

Table 5.32: Comparison of simulation results at different locations for Case 6

	R(0)	R(50)	R(100)	R(150)	R(200)
	Displacement (mm)				
Ls-Dyna	84.22	76.08	58.17	40.71	20.59
Developed Code	84.20	76.06	58.16	40.74	20.62
Difference (mm)	0.02	0.02	0.01	0.03	0.03
	Equivalent Von Mises Stress (MPa)				
Ls-Dyna	1446.22	1396.35	1287.02	1169.35	1123.53
Developed Code	1442.44	1284.76	1261.18	1134.25	1067.30
Difference (MPa)	3.78	111.59	25.84	35.10	56.23

	Effective Plastic Strain (%)				
Ls-Dyna	24.46	21.42	15.92	9.53	6.72
Developed Code	24.39	21.37	15.91	9.47	6.61
Difference	0.07	0.05	0.01	0.06	0.11

CHAPTER 6

CONCLUSION

In this study, a nonlinear explicit finite element program is developed for the purpose of investigating large deformation elastic plastic response of shell structures under impulsive loading. Results of the developed code are compared with Ls-Dyna program simulations and previous experimental study taken from literature. As an outcome of this study following results are concluded:

1. Parametric study showed that bilinear elastic plastic model can capture the deformation behavior accurately.
2. Since the developed code uses predefined blast pressure history as input, numerical errors of calculated pressure history have influence on the developed code results.
3. Material properties may be different between the one used in the experiments and the one used in the simulations which can cause deviation from the test results. In addition, there may be errors in the experiment which stem from measurement errors which are frequently encountered in the high intensity loading conditions.

4. When the outcomes of parameter study for element types are investigated it is concluded that different types of elements including quadrilateral, default triangular (collapsed quadrilateral), triangular with 3rd formulation and triangular with 4th formulation gave similar results. !!!
5. As a result of parameter study, it can be stated that 10 mm element size is sufficient for accuracy without high computational cost for this particular problem.
6. It is observed that 4 integration points through the thickness is sufficient.
7. The average difference between simulations and experimental data is about %10. Finite element simulations over predicted the deformations for the six cases.
8. When the results of the developed code are compared with the experimental data it is concluded that the simulation results are in good agreement with the test results.

For the future study; quadrilateral elements can be implemented in the developed program for more flexibility, more sophisticated plasticity formulation can be implemented, material models considering strain rate effects can be added, blast loading routine can be directly employed to the program to eliminate the dependence on Ls-Dyna software and element failure and erosion can be added.

REFERENCES

[1] Jonas A. Zukas, *Introduction to Hydrocodes*.: Elsevier, 2004.

[2] Woei Shyan Lee, Tao Hsing Chen, and Hsin Hwa Hwang, "Impact Response and Microstructural Evolution of Biomedical Titanium Alloy under Various Temperatures," *Metallurgical and Materials Transactions*, vol. 39, pp. 1435-1448, June 2008.

[3] Stefan Josef Hiermaier, *Structures Under Crash and Impact*.: Springer, 2008.

[4] Alan J. Watson, "Loading from explosions and impact," in *Dynamic Loading and Design of Structures*.: Spon Press, 2002, ch. 6.

[5] G. Le Blanc, M. Adoum, and V. Lapoujade, "External Blast Load on Structures – Empirical Approach," in *5th European LS-DYNA Users Conference*.

[6] Jaroslav Mackerle, "Finite Element Linear and Nonlinear, Static and Dynamic Analysis of Structural Elements: A Bibliography," *Engineering Computations*, vol. 14, no. 4, pp. 347-440, 1997.

[7] Ted Belytschko, Wing Kam Liu, and Brian Moran, *Finite Elements for Nonlinear Continua and Structures*. Wiley, 1996.

[8] Jean Louis Batoz, Klaus Jorgen Bathe, and Lee Wing Ho, "A Study of Three-Node Triangular Plate Bending Elements," *International Journal for Numerical Methods in Engineering*, vol. 15, pp. 1771-1812, 1980.

[9] T. Belytschko and B. J. Hsiehs, "Non-Linear Transient Finite Element Analysis with Convected Co-Ordinates," *International Journal for Numerical Methods in Engineering*, vol. 7, pp. 255-271, 1973.

[10] Ted Belytschko and et al, "Efficient Large Scale Non-linear Transient Analysis by Finite Elements," *International Journal for Numerical Methods in Engineering*, vol. 10, pp. 579-596, 1976.

[11] H. Stolarski, T. Belytschko, and N. Carpenter, "A C0 Triangular Plate Element with One Point Quadrature ," *International Journal for Numerical Methods in Engineering*, vol. 20, pp. 787-802, 1984.

[12] Fred Van Keulen and Jan Booij, "Refined Consistent Formulation Of A Curved Triangular Finite Rotation Shell Element," *International Journal for Numerical Methods in Engineering*, vol. 36, pp. 2803-2820, 1996.

[13] Y. K. Cheung and Y. X. Zhang, "A Refined Nonlinear Nonconforming Triangular Plate Shell Element," *International Journal for Numerical Methods in Engineering*, vol. 56, p. 2387–2408, 2003.

[14] Nicholas Carpenter, Henryk Stolarski, and Ted Belytschko, "A Flat Triangular Shell Element with Improved Membrane Interpolation," *Communications in Applied Numerical Methods*, vol. 1, pp. 161-168, 1985.

[15] T J Hughes and W K Liu, "Nonlinear Finite Element Analysis of Shells. Part I: Three dimensional Shells," *Computational Methods in Applied Mechanics and Engineering*, vol. 26, p. 331–362, 1981.

[16] John O. Hallquist, *LS-DYNA Theory Manual*. Livermore, 2006.

[17] Francis Sabourin and Michel Brunet, "Detailed Formulation of the Rotation-free Triangular Element “S3” for General Purpose Shell Analysis," *Engineering Computations*, vol. 23, no. 5, pp. 469-502, 2006.

[18] E. Onate, P. Cendoya, and J. Miquel, "Nonlinear Explicit Dynamic Analysis of Shells using the BST Rotation Free Triangle," *Engineering Computations*, vol. 19, no. 2, pp. 662-706, 2002.

[19] Shen Wu, Guangyo Li, and Ted Belytschko, "A DKT shell element for dynamic large deformation analysis," *communications in Numerical Methods in Engineering*, vol. 21, pp. 651-674, 2005.

[20] M. Ashgar Bhatti, *Advanced Topics in Finite Element Analysis of Structures*.: Wiley, 2006.

[21] Timothy M. Whalen, *CE 595 Course Notes*.

[22] D.P. Flanagan and L.M. Taylor, *An accurate numerical algorithm for stress integration with finite rotations*.: Computer Methods in Applied Mechanics and Engineering, 1986.

[23] Ted Belytschko, Wing Kam Liu, and Brian Moran, *Nonlinear Finite Elements for Continua and Structures*.: Wiley, 2000.

[24] David J. Benson, "Computational Methods in Lagrangian and Eulerian Hydrocodes," San Diego, 1990.

[25] M.A. Crisfield, *Non-linear Finite Element Analysis of Solids and Structures Volume 2:Advanced Topics*.: Wiley, 2000.

[26] Detlev Maurer, "Rate defined Stress Update applied to Explicit Time Integration Methods," 2003.

[27] Bill Rider, "A Very Brief History of Hydrodynamic Codes," Sandia National Laboratories,.

[28] Seshu Nimmala, "A comparison of DYNA3D, NIKE3D and LS-DYNA Programs," LLNL, 2004.

[29] Livermore Software Technology Corporation (LSTC), *LS-Dyna Keyword User`s Manual*. Livermore, 2007.

[30] Hans U. Mair, "Hydrocode Methodologies for Underwater Explosion Structure/Medium Interaction," in *66th Shock and Vibration Symposium,* 1995, pp. 227-248.

[31] D. P. Flanagan and Ted Belytchko, *A Uniform Strain Hexahedron and Quadrilateral with Orthogonal Hourglass Control*., 1981.

[32] Klaus Weimar, *LS-DYNA User's Guide*.: CAD-FEM GmbH, 2001.

[33] R. C. Hibbeler, *Mechanics of Materials*.: Prentice Hall, 2005.

[34] Vili Panov, *Modelling of Behaviour of Metals at High Strain Rates, PHd Thesis*.: Cranfield University, 2005.

[35] S. S. Akarca, W. J. Altenhof, and A. T. Alpas, "A Coupled Thermal and Mechanical Model of Sliding Wear," in *9th International LS-DYNA Users Conference*, Michigan, 2006.

[36] Microsoft Visual C#.NET Express Edition, *http://www.microsoft.com/express/Downloads/#2008-Visual-CS*., Last Acces Date: January 2010.

[37] DnAnalytics Home Page, *http://www.codeplex.com/dnAnalytics*., Last Access Date: January 2010.

[38] Shen Rong Wu and Weifeng Qiu, "Nonlinear transient dynamic analysis by explicit finite element with iterative consistent mass matrix," *Communications in Numerical Methods in Engineering*, vol. 25, pp. 201-217, 2009.

[39] S. S. Quek. G. R. Liu, *The Finite Element Method: A Practical Course*. Oxford: Butterworth-Heinemann, 2003.

[40] Carmelo Militello and Carlos Felippa, "The First ANDES Elements:9-DOF Plate Bending Triangles," University of Colorado, CU-CSSC-89-22, 1989.

[41] G. R. Liu and S. S. Quek, *The Finite Element Method: A Practical Course*.: Butterworth-Heinemann, 2003.

[42] Ala Tabiei and Romil Tanov, "A nonlinear higher order shear deformation shell element for dynamic explicit analysis: Part I. Formulation and "nite element equations," *Finite Elements in Analysis and Design*, vol. 36, pp. 17-37, 2000.

[43] A. Neuberger, S. Peles, and D. Rittel, "Scaling the response of circular plates subjected to large and close-range spherical explosions. Part I: Air-blast loading," *International Journal of Impact Engineering*, vol. 34, p. 859–873, 2007.

[44] Victor E. Saouma, *Lecture Notes in Finite Element II: Solid Mechanics*.: University of Colorado, 2001.

[45] Antonius Henricus van den Boogaard, *Thermally Enhanced Forming of Aluminium Sheet Modelling and Experiments, PhD Thesis*.: Universiteit Twente, 2002.

[46] Beom-Soo Kangc, Jeong Kim, Sang-Woo Kim, and Woo-Jin Song, "Analytical and numerical approach to prediction of forming limit in tube hydroforming," vol. 47, 2005.

[47] Chen, Y-M; Ruff, A.W; Dally, C.W, *A hybrid method for determining material properties from instrumented micro-indentation experiments*.: Journal of Materials Research, 1994, vol. 9.

[48] Ted Belytschko, J I Lin, and C S Tsay, "Explicit Algorithms for the Nonlinear Dynamics of Shells," *Computer Methods in Applied Mechanics and Engineering*, vol. 42, p. 225–251, 1984.

[49] M. A. Crisfield, G. Jelenic, Y. Mi, H. G. Zhong, and Z. Fan, "Some aspects of the nonlinear finite element method," *Finite Elements in Analysis and Design*, vol. 27, pp. 19-40, 1997.

APPENDIX A

GRAPHICAL USER INTERFACE OF THE DEVELOPED CODE

Graphical user interface contains four major parts (Figure A1):

- Input parameters and solution controls
- Mesh display screen
- Uniform pressure application interface (Figure A2)
- Output messages screen

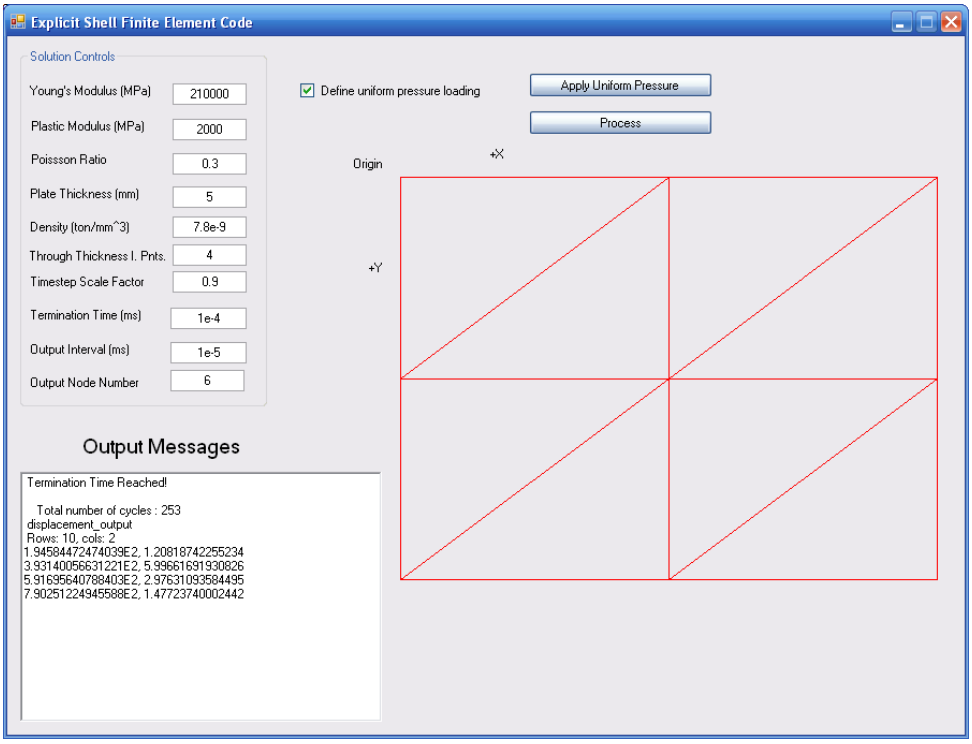

Figure A1: Main window of the developed code

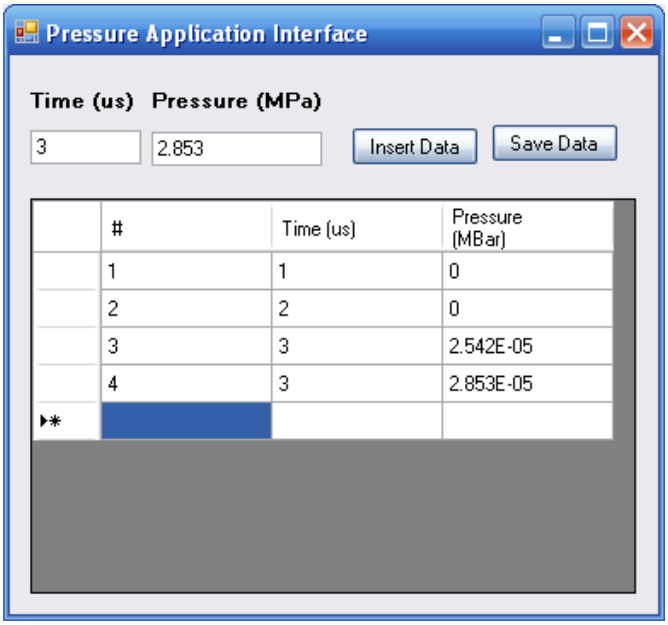

Figure A2: Pressure application interface

APPENDIX B

FLOWCHART OF THE DEVELOPED CODE

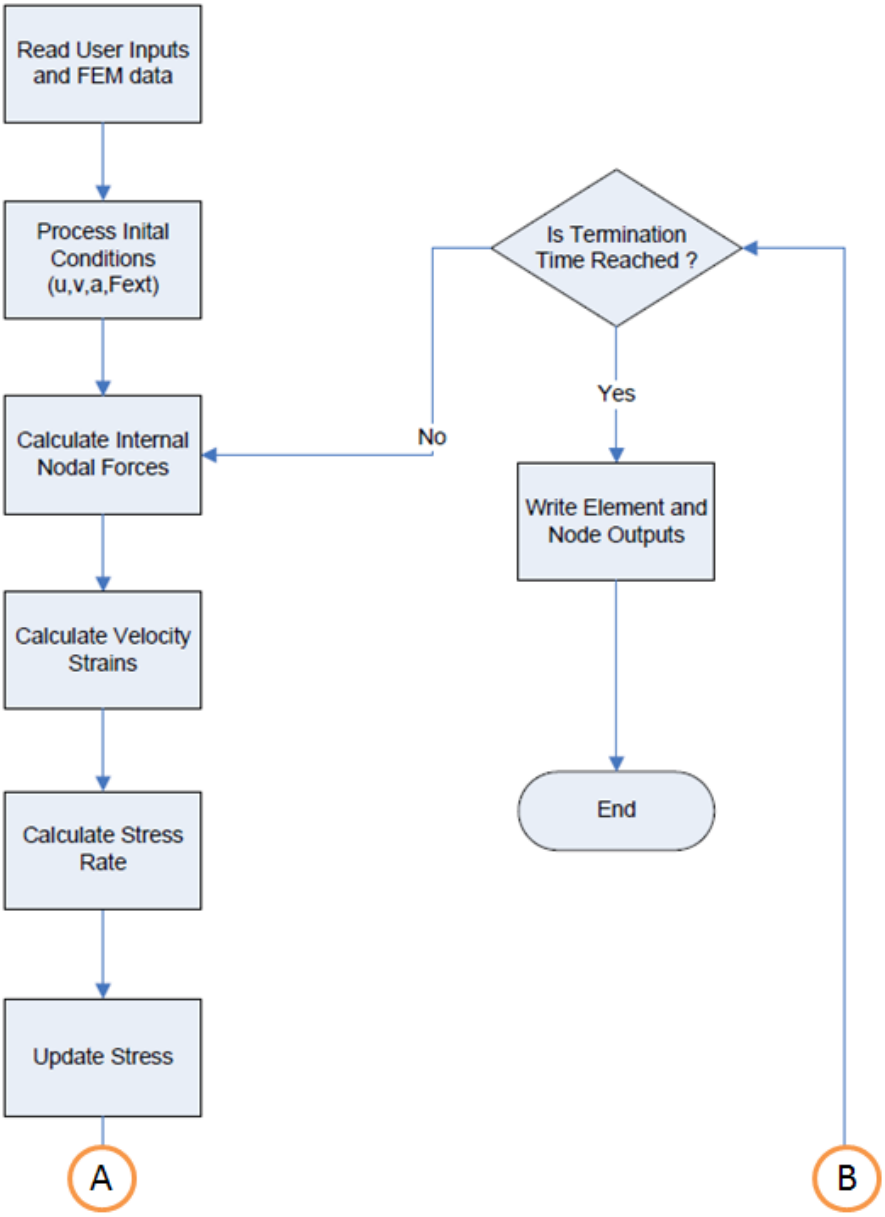

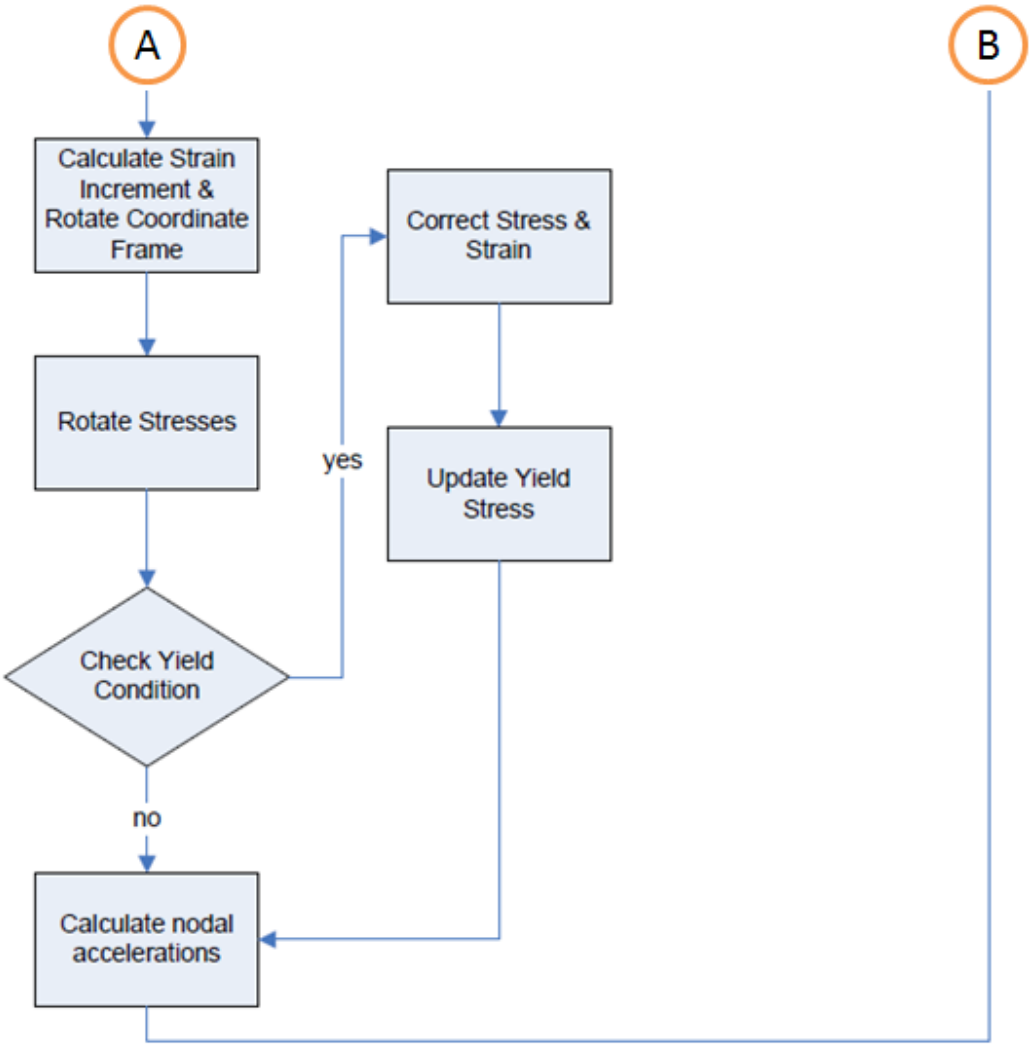

Figure B1: Flowchart of the developed code

APPENDIX C

INPUT FILE FORMAT OF THE DEVELOPED CODE

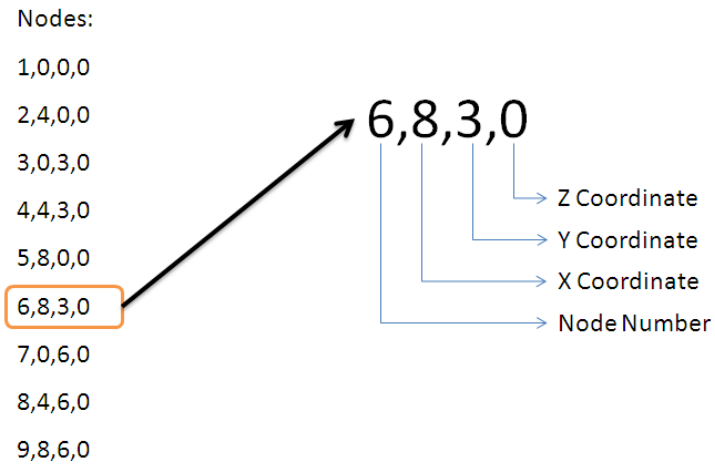

Figure C1: Nodal definitions

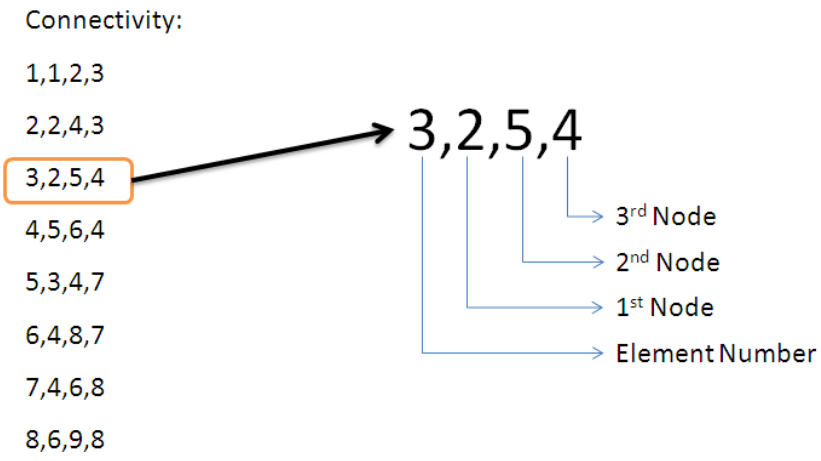

Figure C2: Definition of element connectivity

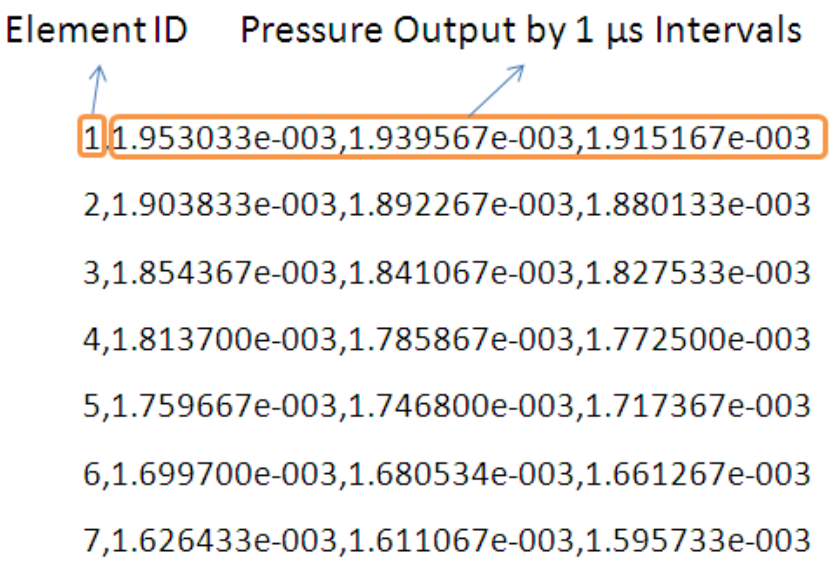

Figure C3: Pressure data taken as time history from Ls-Dyna

APPENDIX D

SAMPLE LS-DYNA KEYWORD FILE

Sample Ls-Dyna input file for second experimental configuration is given below. Nodal data, connectivity and set definitions are removed for simplicity.

```
*KEYWORD
*TITLE
ELFORM 4 mesh 10 mm
*CONTROL_TERMINATION
$#  endtim    endcyc     dtmin    endeng    endmas
 2000.0000         0     0.000     0.000     0.000
*DATABASE_BINARY_BLSTFOR
$#      dt      lcdt      beam     npltc    psetid
  1.000000         0         0         0         0
*DATABASE_BINARY_D3PLOT
$#      dt      lcdt      beam     npltc    psetid
 10000.000         0         0         0         0
$#   ioopt
         0
*DATABASE_HISTORY_NODE
*BOUNDARY_SPC_NODE
$#     nid       cid      dofx      dofy      dofz     dofrx
dofry     dofrz

*LOAD_BLAST_ENHANCED
         1 468.00000     0.000     0.000 100.00000     0.000
4         2
     0.000     0.000     0.000     0.000         01.0000E+20
*LOAD_BLAST_SEGMENT_SET
$#     bid      ssid    alepid
         1         1         0
*PART
$#     pid     secid       mid     eosid      hgid      grav
adpopt      tmid
         1         1         2         0         0         0
```

```
*SECTION_SHELL
$#   secid    elform      shrf       nip     propt   qr/irid
icomp     setyp
         1         4     0.000         4         1         0
0         1
$#      t1        t2        t3        t4      nloc     marea
idof    edgset
  1.000000  1.000000  1.000000  1.000000     0.000     0.000
0.000         0

*BOUNDARY_SPC_NODE
$#     nid       cid      dofx      dofy      dofz     dofrx
dofry     dofrz

*LOAD_BLAST_ENHANCED
$#     bid         m       xbo       ybo       zbo       tbo
unit     blast
         1 468.00000     0.000     0.000 100.00000     0.000
4         2
$#     cfm       cfl       cft       cfp     nidbo     death
     0.000     0.000     0.000     0.000         01.0000E+20
*LOAD_BLAST_SEGMENT_SET
$#     bid      ssid    alepid
         1         1         0
*PART
$# title
Part number 1
$#     pid     secid       mid     eosid      hgid      grav
adpopt      tmid
         1         1         2         0         0         0
0         0
*SECTION_SHELL
$#   secid    elform      shrf       nip     propt   qr/irid
icomp     setyp
         1         4     0.000         4         1         0
0         1
$#      t1        t2        t3        t4      nloc     marea
idof    edgset
  1.000000  1.000000  1.000000  1.000000     0.000     0.000
0.000         0
```

```
*MAT_PLASTIC_KINEMATIC_TITLE
RHA_bilinear
$#     mid         ro          e         pr       sigy       etan
beta
         2   7.800000   2.100000   0.300000   0.010000   0.020000
0.000
$#     src        srp         fs         vp
     0.000     0.000     0.000     0.000
*DEFINE_CURVE
$#    lcid       sidr        sfa        sfo       offa       offo
dattyp

*SET_SEGMENT
$#     sid        da1        da2        da3        da4
         1     0.000     0.000     0.000     0.000
$#      n1         n2         n3         n4         a1         a2
a3        a4
*ELEMENT_SHELL
*NODE
*END
```